Noncovalent interactions of molecules with single walled carbon nanotubes

David A. Britz[ab] and Andrei N. Khlobystov*[c]

In this *critical review* we survey non-covalent interactions of carbon nanotubes with molecular species from a chemical perspective, particularly emphasising the relationship between the structure and dynamics of these structures and their functional properties. We demonstrate the synergistic character of the nanotube–molecule interactions, as molecules that affect nanotube properties are also altered by the presence of the nanotube. The diversity of mechanisms of molecule–nanotube interactions and the range of experimental techniques employed for their characterisation are illustrated by examples from recent reports. Some practical applications for carbon nanotubes involved in non-covalent interactions with molecules are discussed.

1. Introduction

Carbon nanotubes (NTs) are hollow cylindrical tubes with diameters ranging between 1 and 100 nm. The idealised wall of a NT cylinder is made of one or more concentric sheets of sp^2 carbons.[1] NTs made of one graphene sheet generally are narrower, ranging from 0.4 nm to 3 nm[2,3] in diameter, and are referred to as single-walled nanotubes (SWNTs). The diameter, curvature, and electronic properties of a nanotube are uniquely defined by the way hexagonal rings constituting the nanotube sidewall are joined together, which is referred to as nanotube chirality (Fig. 1). For an extended discussion of nanotube structure and physical properties, see reference 1.

[a]Department of Materials, University of Oxford, Parks Road, Oxford, UK OX1 3PH
[b]Eikos Inc., 2 Master Drive, Franklin, MA 02038, USA
[c]School of Chemistry, University of Nottingham, University Park, Nottingham, UK NG7 2RD.
E-mail: andrei.khlobystov@nottingham.ac.uk; Fax: 0115 9513563

Nanotubes have a rich and interesting history that spans virtually all scientific disciplines. It is commonly stated that NTs were accidentally discovered in 1991 by Iijima[4] in the insoluble material of arc-burned graphite rods. This technique was well-known to produce the famed Buckminster fullerene on a preparative scale,[5] and this was just one more accidental discovery relating to fullerenes. The original observation of fullerenes in mass spectrometry was not anticipated,[6] and the first mass-production technique by Kratchmer and Huffman was used for several years before realising that it produced fullerenes.[5]

It seemed fitting that nanotubes were also serendipitously discovered. However, a paper by Oberlin, Endo, and Koyama published in 1976 clearly showed hollow carbon fibres with nanometer-scale diameters using a vapour-growth technique.[7] Also, in 1987, Tennent of Hyperion Catalysis was issued a US patent for the production of "cylindrical discrete carbon fibrils" with a "constant diameter between about 3.5 and about 70 nanometers…, length 10^2 times the diameter, [and] an

David A. Britz graduated in 2002 from the University of Virginia with BSc in Mechanical Engineering. He completed his DPhil degree at the Department of Materials, University of Oxford, in 2005. Currently, he is a Senior Engineer at Eikos, Inc in Franklin, Massachusetts, USA. At Eikos, he is working on a Department of Energy project to incorporate carbon nanotube-based Invisicon® films into photovoltaic cells for use as a transparent, conductive elec-

David A. Britz

trode material. His primary interests are in the areas of non-covalent interactions of carbon nanotubes, molecular self-assembly, nanocomposites, and nanostructure–macroscopic property correlation.

Andrei N. Khlobystov received MSc and PhD degrees in Chemistry from Moscow State University (Russia) in 1997 and the University of Nottingham (UK) in 2002, respectively. He then joined the Department of Materials, Oxford University, as a post-doctoral research assistant. He was awarded the Leverhulme Trust Early Career Fellowship in 2004 and the Royal Society University Research Fellowship in 2005. He is currently working as a Research Fellow at the

Andrei N. Khlobystov

School of Chemistry, University of Nottingham. His current research focuses mainly on the chemistry of carbon nanotubes and fullerenes and development of applications for these materials. His other research interests include coordination and supramolecular chemistry and electron microscopy. He has recently received a European Young Investigator Award.
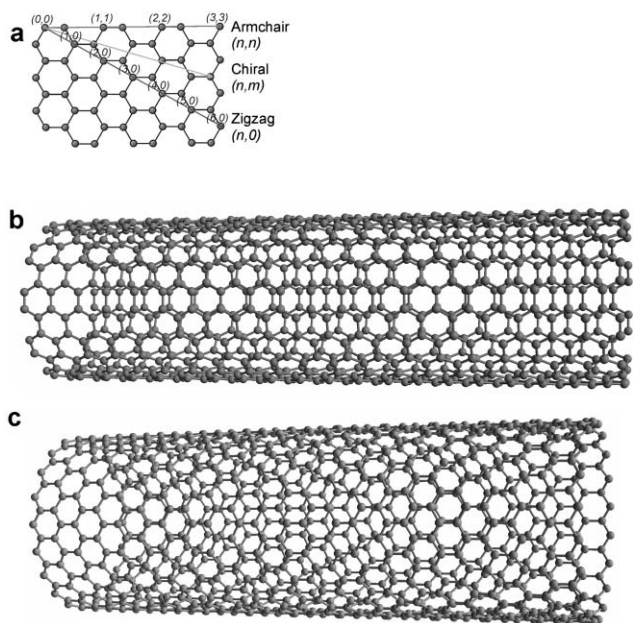
Fig. 1 (a) Wrapping vector of graphene sheet defines the structure (chirality) of carbon nanotubes. Examples of (b) "armchair" and (c) "zigzag" SWNTs.

outer region of multiple essentially continuous layers of ordered carbon atoms and a distinct inner core...."[8] More recently, Endo has been credited with discovering NTs, and Iijima has been credited for elucidating the structure of NTs. Iijima and co-workers[9] and, independently, Bethune and co-workers at IBM[10] controllably grew single-walled carbon nanotubes. The closed end of a nanotube was seen to resemble half of a fullerene, and "buckytubes" were quickly picked up by fullerene researchers.

Carbon nanotubes, especially SWNTs, have been termed "materials of the 21st century" due to their functional mechanical, electrical and optoelectronic properties, since they already outperform classical materials such as organic polymers and semiconductors.[11] Fuelled by potentially important applications for these materials, carbon nanotube research has sprung to an astonishing scale in only a few years, opening new challenges and opportunities for chemistry of these structures. Nanotube research is truly multi- and interdisciplinary: engineers are developing next-generation composites,[12] electronic devices,[11] and adsorbents[13] based on nanotubes; chemists are exploring nanotubes as containers for molecules[14] and ions[15] and as nanoscale reactors; biologists see nanotubes as potential shuttles for organ-selective drug delivery and other therapeutic and diagnostic purposes.[16–18] The physico-chemical nature of carbon nanotubes, which essentially can be viewed as fully conjugated polyaromatic macromolecules with a hollow, inert interior and reactive exterior and ends, drives applications in all these fields.

While fundamental research of nanotubes focuses on the intrinsic properties of isolated carbon nanotubes, applications heavily rely on interactions of NTs with their environment. These interactions can be manifested in various non-covalent forces acting between the nanotube and molecular, ionic or macromolecular species constituting the nanotube environment. Due to their high polarizability and smooth surface, SWNTs form strong van der Waals interactions between each other reaching ~ 500 eV per 1 μm of NT's length[19] and aggregate into bundles and ropes where several nanotubes are aligned parallel to each other forming a triangular array (Fig. 2).[20] Substantial effort is required to break bundles so that individual nanotubes can be studied. Because additions of chemical groups to the nanotube sidewall disrupt packing of bundles, it becomes easier to disperse functionalised nanotubes in solvents,[21] a distinct advantage of adding functionality, though changes to nanotube properties caused by covalently attached groups can be dramatic, permanent, and are not always controllable. Adding any covalent functionality to the nanotube inevitably changes the nanotube electronic structure; controlling functionality is of substantial interest and has been reviewed recently.[22] If one wishes to reversibly alter or finely tune nanotube properties, molecules that interact via ionic and dispersive bonding appear to be good candidates.

Here we survey the field of noncovalent interactions between molecules and nanotubes. We demonstrate the synergistic character of the nanotube–molecule interactions, as molecules that affect nanotube properties are also altered in the presence of the nanotube. The diversity of mechanisms of molecule–nanotube interactions and the range of experimental techniques employed for their characterisation are illustrated by examples from recent reports. Some practical applications for carbon nanotubes involved in non-covalent interactions with molecules are discussed.
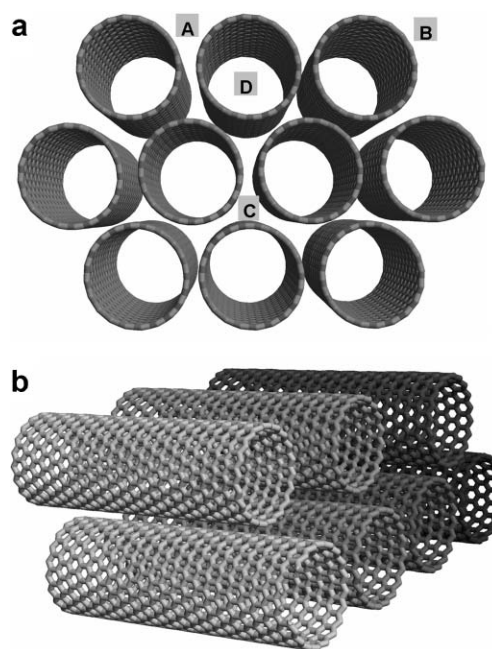

Fig. 2 Schematic diagram of a bundle of nanotubes (a) cross-section view and (b) side view. Possible adsorption sites for small molecules: grooves of bundles – A, outer surface of sidewalls – B, interstitial cavities – C, and nanotube cavities – D.

2. SWNT exterior *versus* interior

Although carbon nanotubes and graphite are built of the same basic units, hexagons of sp^2-hybridised carbon atoms, and considered to be close relatives, there is a substantial difference between physico-chemical properties of these materials. The character of C–C bonds in nanotubes differs from that of graphite as the carbon atoms in a nanotube are pyramidalized due to the curvature of the nanotube sidewall (Fig. 3).[23] A (10,10) and (5,5) nanotube have a pyramidalization angle of $\theta_p = 3.0°$ and $6.0°$, respectively. This pyramidalization gives some of the π-orbitals of C-atoms some σ character and should distort the π orbitals to be larger and softer on the exterior of the nanotube, an effect that has been calculated to give nanotubes an intrinsic p-type semiconducting behaviour.[24]

Curvature in the nanotube introduces misalignment of π-orbitals within the graphene sheet (Fig. 3).[23] The π-orbitals of a nanotube are not pointed directly towards the central axis of the nanotube, and some adjacent carbon π-orbitals have a misalignment angle, ϕ, between them. The π-orbitals of adjacent carbon atoms in a (10,10) and (5,5) nanotube have a π-orbital misalignments for the two different C–C-bonds of $\phi = 0°$ and $10.4°$ for (10,10) and $0°$ and $21.3°$ for (5,5), respectively. Strain in nondefective nanotube sidewalls is manifested in pyramidalization and π-orbital misalignment, which can be relieved by the addition of an atom or functional group to the nanotube exterior.

As the nanotube diameter increases, both the pyramidalization angle and π-orbital misalignment angle decrease, lowering the chemical reactivity of the C–C-bonds, eventually approaching planar graphite for very large NT diameters. As ideal nanotubes are made solely of sp^2-bonded carbon atoms, the covalent addition of an atom, such as fluorine or hydrogen,

to the exterior of a carbon nanotube would change hybridisation of C-atom to sp^3 and would partly relieve strain energy.[25,26] However, addition of an atom to the interior of the sidewall would add strain energy to the nanotube. Theoretical modelling has shown that the interior of a SWNT is more inert than the exterior of a nanotube to the addition of atomic nitrogen,[27] atomic carbon,[28] atomic fluorine,[26] atomic hydrogen,[26] and amidogen.[29] Chen *et al.*[26] calculated that the addition of H and F to the interior of (n,n) SWNTs ($n \geqslant 4$) can be exothermic, though exterior additions are more favourable. Nonetheless, (4,4) SWNTs are small compared to most produced SWNT samples, and therefore it would seem possible that the interior of a SWNT could be involved in chemical reactions if a reactive species is selectively trapped inside. Also, Chen *et al.* showed that endohedral bonding can become substantially more exothermic if it takes place in the direct region where a carbon atom has an exohedral H or F. Thus nanotubes with sidewall defects may be as reactive on the interior as the exterior of a structurally perfect nanotube. Because the SWNT interior reactivity changes with exterior functionalization, we can envisage a reaction where trapped molecules are induced to react by functionalizing the exterior of the SWNT. Alternatively, if reaction with the interior of a nanotube is not desired, then double-walled carbon nanotubes (DWNTs) could be instead of SWNTs. The inner nanotube of DWNTs should have largely unchanged reactivity after functionalizing the exterior nanotube. Experimentally, ozonation of SWNT sidewalls was shown to be diameter selective, with smaller diameters reacting most readily, thus supporting the theory that sidewall reactivity is diameter-dependent.[30]

Bending a graphene sheet increases the reactivity of the convex surface and decreases in reactivity the concave surface,
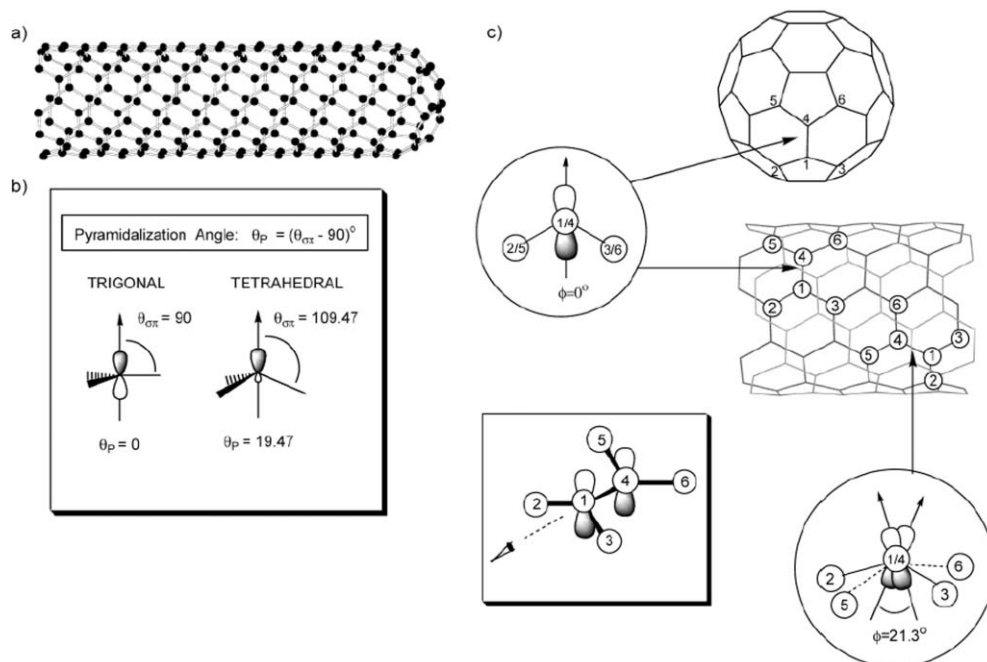

Fig. 3 Diagrams of (a) metallic (5,5) SWNT, (b) pyramidalization angle θ, and (c) the π-orbital misalignment angles ϕ along the C1–C4 in the (5,5) SWNT and its capping fullerene, C_{60}. (Reproduced with permission from ref. 23, copyright 2002 American Chemical Society.)

This journal is © The Royal Society of Chemistry 2006

Chem. Soc. Rev., 2006, **35**, 637–659 | 639

relative to planar graphite for covalent additions. The difference in reactivity is driven by strain and a change in the character of C–C-bonds accompanying strain. This difference implores us to ask if noncovalent bonding (*i.e.* dispersion and ionic interactions) are also different inside and outside of a nanotube.

Recently, Tournus and Charlier[31] theoretically considered the adsorption of benzene on the outside of chiral and armchair SWNTs using DFT methods. They found a surprising result: the adsorption of benzene over the bridge of a C–C bond was strongest for minimal π-orbital misalignment. For a SWNT of 7.28 Å in diameter, the difference in binding energy between C–C-bonds with $\phi = 0°$ and $\phi = 23.0°$ was calculated to be 17 meV, about 9% of the total binding energy. Since π-orbital misalignment ϕ is inversely proportional to diameter, wider nanotubes tend to have a greater binding energy for benzene due to a better geometric match with planar benzene *and* a decrease in π-orbital misalignment. This result implies that dispersive interactions for molecules on SWNTs are fundamentally different depending on the nanotube curvature and π orbital orientation. It is possible that greater differences in dispersive binding exist on the inside and outside of SWNTs due to different π orbital shapes and orientations between the two surfaces.

The curvature of a cylindrical graphene sheet makes the two sides of the sheet different geometrically; the nanotube curves away from a small molecule on the exterior of the nanotube and curves towards a small molecule on the interior of the nanotube. The simplest model for determining interactions of a molecule with a nanotube that can give quantitatively correct results for specific cases is the empirical Lennard–Jones potential (LJP) to describe dispersive (*i.e.* van der Waals) interactions. This empirical model has been successfully applied for graphitic structures,[32] and should be applicable to molecules and atoms adsorbed on SWNTs. To determine energy of binding between a NT and a molecule, interactions between the molecule and each atom of carbon nanotube are summed; the energy of interaction between two atoms is described by the empirical relation: $V_{LJ}(r) = 4\varepsilon\left[\left(\frac{\sigma}{r}\right)^{12} - \left(\frac{\sigma}{r}\right)^{6}\right]$, where r is the distance between atoms, ε is the well depth and σ is the hard sphere radius of the atom. The ε and σ parameters are assigned the same value for the interior and exterior of a SWNT, an assumption that has not been rigorously shown to be true. It

was suggested that an energy correction of 1–2% for curvature could be expected, based on similar corrections for curvature-induced changes in electronic structure,[33] though π orbital misalignment may introduce larger differences in binding energy.[31] Often, rather than using a discrete potential, a continuum approach has been used,[19,32,34–36] where the electronic density is assumed to be uniform over the surface of the nanotube. The continuum and discrete approaches give similar values for energy of interaction, usually within a few percent for most systems.[34,37] If the effect of NT sidewall corrugation is of interest, then the discrete approach is necessary, since a continuum approach cannot reveal anything about the sidewall potential energy surface.

To reveal the qualitative behaviour of an atom interacting with a nanotube, a simplified LJP model can be used, where an arbitrary atom of van der Waals diameter d interacts *via* van der Waals interactions with an arbitrary nanotube bundle made of NTs with diameter D.[38] By only varying D, the binding energy of the atom (or small molecule) on the nanotube changes (Fig. 4). As $D \rightarrow \infty$, the outside and inside of the infinite diameter nanotube are equivalent surfaces (Fig. 4e). The binding energy of the atom to the exterior of the infinite diameter NT is equal to the binding energy on planar graphene. As D is decreased, the binding energy of the atom to the exterior decreases monotonically. The binding energy of the atom inside a nanotube has qualitatively different behaviour when varying the nanotube diameter.

Returning to a NT of $D \rightarrow \infty$, the atom's binding energy on the interior of the NT would be equal to the binding energy on planar graphene. As D is decreased, the binding energy increases, then reaches a maximum binding energy at an ideal NT diameter for that atom (Fig. 4b). This condition occurs when $D = d + 2 \times r_{vdW}$, where r_{vdW} is the thickness of the NT's π orbitals. As the nanotube diameter decreases further, the repulsive component of the LJP becomes dominant due to large overlap of atom and NT orbitals (Fig. 4a). At the ideal diameter of a nanotube for a given molecule (Fig. 4b), the binding energy *strongly* favours the interior site; at larger diameters, the interior site remains favourable (Figs. 4c,d), but less so than at the ideal diameter of $D = d + 2 \times r_{vdW}$. From this simple model, it is clear that the ratio of van der Waals diameter of molecule to NT diameter is the main factor defining the favourable location of the molecule. This model is correct for nanotube–molecule interactions where van der
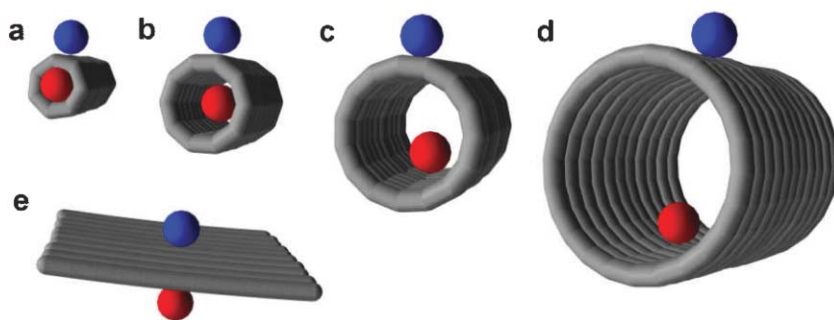

Fig. 4 Schematic diagrams of small molecules exohedrally (blue) and endohedrally (red) adsorbed on nanotubes of different diameters ($d_{molecule}$ is van der Waals diameter of molecule, and d_{NT} is internal van der Waals diameter of nanotube): (a) $d_{NT} < d_{molecule}$, (b) $d_{NT} \sim d_{molecule}$, (c) $d_{NT} > d_{molecule}$, (d) $d_{NT} \gg d_{molecule}$, (e) $d_{NT} = \infty$.

Waals forces are dominant, which makes this model applicable for many of the examples described in this review.

The potential energy surfaces (PES) for an adatom on zig-zag and armchair SWNTs were calculated using a Tersoff–Brenner many-body potential for carbon atoms and a LJP for interaction between the adatom and the carbon atoms.[39] It was found that curvature substantially affects the PES of a graphene sheet. The interior of zig-zag and armchair nanotubes have a smoother PES than graphite, and graphite has a smoother PES than the exterior of a nanotube. While the interaction energy of an adatom on the interior of a nanotube is greater than on the exterior, the barrier for diffusion is lower inside the nanotube. The relative smoothness of the interior PES is likely due to the compression of the π-orbitals due to the bent graphene sheet. Understanding the smoothness of the PES is also important for molecular transport and fluid flow, since a smoother PES would reduce transport and diffusion barriers.

A recent paper[40] reported the calculated energy of adsorbing a lithium adatom endohedrally and exohedrally on SWNTs. The authors found an energy gain of 2.33 eV for endohedral adsorption and 2.17 eV for exohedral adsorption of lithium on a (5,5) SWNT. They found that a full transfer of one electron occurs from the Li to the SWNT in both cases. The authors also calculated that endohedral lithium has a lower diffusion barrier than exohedral lithium by as much as 100 meV due to a much smoother endohedral PES. Lu et al.[41] calculated that potassium atoms have donated essentially one full electron to a SWNT bundle in cases when K is located in interstitial and endohedral sites. They also found a binding energy for the stoichiometry KC_{80} of 2 eV for interstitial binding and 1 eV for endohedral binding. It is not fully clear if the difference in binding energy is due to the higher coordination number of K in the interstitial sites or to electronic effects. While intuition would lead us to believe that charge transfer is equally likely for a molecule or atom inside a SWNT as it is outside a SWNT, this prediction has yet to be investigated experimentally.

As demonstrated in the next section, it can be rather difficult to distinguish experimentally between the endohedral and exohedral adsorption of small molecules from the gas phase, which form highly dynamic, reversible interactions with nanotubes and so both scenarios (interior and exterior adsorption) are considered within this section. However the interactions of NTs with larger molecules can be clearly divided into two categories: "molecules outside nanotube" and "molecules inside nanotube" which are discussed in sections 3.2 and 4 respectively.

3. Interaction of molecules with the exterior of nanotubes

Bundles of as-produced unprocessed SWNTs present several adsorption sites for molecules: the interstitial sites C (Fig. 2a), the groove of two intersecting SWNTs on the surface A, and the exterior surface of single nanotube B. Each site has progressively weaker bonding to a small molecule due to a decrease in number of interacting carbon atoms. For a larger molecule, interstitial sites are no longer favourable, since the

nanotubes of the bundle would have to separate to allow a molecule to intercalate. Defects in nanotube sidewalls and end-caps make the interior of SWNTs D (Fig. 2a) accessible for molecules. This is especially important for HiPCO SWNTs, which are produced with a percentage of the nanotubes opened and with the interior accessible for filling.[42,43]

3.1. Gas phase

Eswaramoorthy et al. were among first to study the adsorption of gases onto SWNTs. They showed that SWNTs have a high surface area of ca. 400 m^2 g^{-1} using BET N_2 absorption isotherms at 77 K.[44] They demonstrated that treatment with concentrated HCl increased the surface area of SWNTs, making the interior cavity more accessible. Strengthening their conclusion, they calculated the maximum of the pore size distribution to be 11 Å which is in agreement with the nanotube average diameter in this sample. They also showed that both benzene and methanol adsorb on SWNTs, more so on HNO$_3$-treated samples. It is well-demonstrated that HNO$_3$-treatment opens nanotubes and creates sidewall defects,[21,45] which explains the increased adsorption of the organic molecules on HNO$_3$-treated nanotubes. However, it is also possible that the increase of benzene and methanol adsorption resulted from a relative weight increase in SWNTs in the sample due to removal of catalyst and amorphous carbon, as well as dispersion of large bundles during HNO$_3$-treatment. This result emphasizes the difficulty of deducing the location of small molecules adsorbed on SWNTs using a single technique.

Teizer et al. studied the energetics of noble gas adsorption on SWNTs. They reported that thermal desorption measurements of ^{4}He from SWNTs gave a binding energy 150% greater than ^{4}He on planar graphite,[46] but they found that their temperature calibration was incorrect, restating the binding energy of ^{4}He on SWNTs to be 60% greater than ^{4}He on planar graphite.[47] Since these nanotubes were purified, it is likely that the interiors were accessible for adsorption, and the experimentally determined binding energy for ^{4}He would imply adsorption on groove sites of bundles and inside SWNT cavities. It was found experimentally that Ne,[48] Xe,[49] and CH$_4$[50] adsorb only on groove sites with a binding energy 75% greater than the respective molecule on planar graphite. No adsorption in interstitial channels was observed, even though Ne should have a size small enough to fit inside interstitial channels.[48] The observed increase in adsorption energies for small molecules on SWNTs as compared to graphite is in line with theoretical calculations.[38] Another study has reported that the binding energy of Xe in groove sites is 25% higher than that for planar graphite, which is also supported with calculations.[51] Interestingly, the values for Xe binding energy are the same for references 51 and 49, but the value for Xe binding on planar graphite is different.

A recent theoretical study of adsorption of gases on heterogeneous bundles (i.e. comprising nanotubes with different diameters) shows that interstitial channels are larger than for homogeneous bundles, and large enough to incorporate all of the above gases.[52] They find excellent matches for experimental heats of adsorption for heterogeneous bundles,

This journal is © The Royal Society of Chemistry 2006

Chem. Soc. Rev., 2006, **35**, 637–659 | 641

whereas homogeneous bundles do not match experiments well. However, direct experimental evidence for adsorption in interstitial channels is lacking, possibly due to the insensitivity of experimental methods.

For bundles of open-ended SWNTs, the predominant adsorption site for Ar was found to be inside the SWNT cavity, followed by groove sites. Interstitial adsorption was found to be limited, since neutron diffraction patterns were dominated by Ar atoms adsorbed on endohedral and groove sites of nanotube bundles.[53] These reports showed that a substantial amount could be learned by examining the energetics of adsorption and desorption experimentally and theoretically. However, due to the difficulty of studying individual SWNTs and the ease with which small molecules desorb, direct evidence of small molecule encapsulation inside SWNTs was lacking for many years.

Infrared (IR) spectroscopy has proved to be a very sensitive technique to study different adsorption sites on SWNTs. For gas molecules adsorbed onto SWNT surfaces, there is a dispersive interaction that causes a softening of the bonds in the molecule, seen as a downshift (i.e. red shift) in IR modes (Table 1). This effect has been well-documented and has been used to distinguish between exohedral and endohedral adsorption by magnitude of the shift.[54] This difference was shown with clarity and supported by calculations for CO_2 adsorbed on SWNTs. The $v(C–O)$ mode of endohedral CO_2 showed a downshift Δ of 8 cm⁻¹ and the exohedral CO_2 showed a downshift of 3 cm⁻¹, compared to the gas phase. For physisorbed molecules, the higher coordination of endohedral sites causes a greater downshift for endohedrally adsorbed gas molecules, compared to groove sites on the surface of bundle (Table 1).

In most cases, non-covalent interactions with nanotubes affect adsorbed molecules only slightly and are manifested in moderate downshifts of vibration frequencies of the molecules by 10–35 cm⁻¹. However, there are some notable examples of particularly large IR shifts of molecules adsorbed onto SWNTs such as H_2O,[57] NH_3,[57] and NO_2[57] which exhibit IR downshifts of 100 cm⁻¹ or greater for some modes when interacting with SWNTs. Though HiPCO SWNTs were shown to have a high percentage (17–40%, varying with different batches) of SWNTs open prior to any treatment,[42,43] Ellison et al. do not take into account the possibility of endohedral adsorption for any of these molecules. For H_2O adsorption at room temperature,[57] they found that their IR peaks were well-fit by two Lorentzian lines of 3255 and 3390 cm⁻¹. Liquid H_2O has two stretch modes at 3280 and 3490 cm⁻¹, showing a large shift of these modes, potentially indicating a more substantial interaction between H_2O and SWNTs than for small gas molecules or an altered H_2O–H_2O interaction due to confinement. They noted that a small percentage of the H_2O molecules react with the nanotubes, presumably at defect sites, to form C–O bonds. It has been calculated that H_2O will disproportionate to H_2 and O_2 at much lower energy in the presence of a pentagon–heptagon defect on the SWNT sidewall.[61] Further experimental and theoretical investigations could reveal that SWNTs would make ideal catalysts for a variety of reactions.

For NH_3 adsorption at room temperature,[57] Ellison et al. found shifts of −180 and −131 cm⁻¹ for the symmetric stretch, −165 and −96 cm⁻¹ for the asymmetric stretch, and −11 cm⁻¹ for the bend mode. In other studies, a splitting of IR peaks was assigned to two different environments,[54] specifically endohedral and exohedral adsorption sites.[42,56] It is not clear if the splitting of symmetric and asymmetric stretch modes of NH_3 are due to different adsorption sites, but this effect could be studied systematically by varying sample treatment. For the two umbrella modes, shifts of +386, and +316 cm⁻¹ were seen for the two peaks, ascribed to interaction of the nitrogen lone pair of electrons with the SWNT. The softening of some NH_3 modes and the hardening of the umbrella mode indicates an interaction with SWNTs that is dispersive with the hydrogen atoms and donor–acceptor (largely covalent) with the nitrogen atom. As discussed previously, covalent bonding is strongly favoured on the SWNT exterior, so it would follow that ammonia would tend to bond to the exterior of the SWNT with covalent character, but it would have a largely dispersive interaction with the interior of the SWNT. Since dispersive interactions favour endohedral adsorption, it is possible that the splitting of the stretch peaks is due to endohedral and exohedral adsorption on partially opened HiPCO SWNTs. The binding of ammonia was shown to be strong (which could be a result of effective donor–acceptor interactions) by thermal desorption measurements, where NH_3 begins to substantially desorb at 400 K. In contrast, the boiling point of liquid NH_3 is at 240 K. A very recent work[60] ascribes the room temperature adsorption and high temperature desorption of NH_3 observed by Ellison et al. to defects possibly serving as chemisorption sites in HiPCO SWNT samples. They find IR peak positions that are virtually identical to condensed phase IR modes of NH_3,[60] an appropriate comparison since SWNT IR measurements were

Table 1 Effects of interactions with nanotubes on IR spectra of small molecules

Molecule	Non-interacting I/cm⁻¹	Endohedral I/cm⁻¹	Exohedral I/cm⁻¹	Endohedral Shift I/cm⁻¹	Non-interacting II/cm⁻¹	Endohedral II/cm⁻¹	Exohedral II/cm⁻¹	Endohedral Shift II/cm⁻¹
CO[42]	v = 2143 (gas)	v = 2135	v = 2140	Δ = −8	—	—	—	—
(NO)$_2$[55]	v_1 = 1868 (gas)	v_1 = 1853	—	Δ = −15	v_5 = 1789 (gas)	v_5 = 1754	—	Δ = −35
CO$_2$[54]	v = 2349 (gas)	v = 2329	v = 2342	Δ = −20	—	—	—	—
SF$_6$[56]	v_3 = 947 (gas)	v_3 = 927	—	Δ = −20	—	—	—	—
H$_2$O[57]	v_{ss} = 3280(liq)	v_{ss} = 3255	v_{ss} = 3255	Δ = −25	v_{as} = 3490 (liq)	v_{as} = 3390	v_{as} = 3390	Δ = −100
CF$_4$[58]	v_3 = 1282 (gas)	v_3 = 1247	v_3 = 1267	Δ = −35	—	$2v_4$ = 1258	$2v_4$ = 1257	—
H$_8$Si$_8$O$_{12}$	v(Si–H) = 2277 (solution)	v(Si–H) = 2262	—	Δ = −15	—	—	—	—
NH$_3$[59]	v_1 = 3336 (gas)	v_1 = 3156	v_1 = 3205	Δ = −180	v_3 = 3414 (gas)	v_3 = 3249	v_3 = 3318	Δ = −165
NH$_3$[60]	v_1 = 3290(liq)	v_1 = 3290	v_1 = 3290	Δ = 0	v_3 = 3378 (liq)	v_3 = 3376	v_3 = 3376	Δ = −2
NO$_2$[59]	v_{ss} = 1318 (gas)	v_{ss} = 1026	v_{ss} = 1026	Δ = −292	v_{as} = 1618	v_{as} = 1302	v_{as} = 1302	Δ = −316

made at 94 K. This result is surprising because NH_3 adsorbed onto fullerenes have greater IR shifts than on SWNTs, compared to the condensed phase, even though both sp^2 carbon structures would be expected to affect NH_3 similarly.

NO_2[57] adsorbed onto HiPCO SWNTs at room temperature does not show a splitting of IR modes, though the observed peaks are broad. Like in the case of NH_3, the authors observe large shifts of symmetric and asymmetric modes of -292 and $-316\ cm^{-1}$, respectively for adsorbed NO_2. The bending mode was seen to shift by $+58\ cm^{-1}$. They observed shifts similar to those measured for NO_2 chemisorbed on a metal surface. Yim et al.[65] reported a theoretical study showing that two NO_2 molecules per nanotube supercell chemisorb onto the exterior wall of a perfect (8,0) SWNT using DFT calculations. This observation is interesting because one NO_2 molecule per SWNT supercell weakly bonds (i.e. physisorbs) to an (8,0) SWNT, but the second NO_2 molecule added to the SWNT promotes both molecules to be strongly chemisorbed. Previous theoretical works only considered physisorption of one NO_2 molecule per supercell,[62–64] which was always found to be energetically more favourable than chemisorption of one molecule per supercell.[65] Yim et al. calculated that chemisorption of two molecules is substantially favoured to physisorption, a process that is exothermic by as much as 21.4 kcal mol^{-1} (928 meV). Multiple NO_2 molecules always weakly bond to a unit cell of graphite, showing that curvature of the graphene sheet increases reactivity, though occasionally through less straightforward mechanisms than would be expected. Ellison et al. experimentally observed that NO_2 desorbed at 400 K, indicating a strong binding to the SWNT, rather than a weak physisorption.[59] Yim et al.'s observation that the exterior is more reactive is attributed to curvature of the SWNT and corresponding relief of strain by forming a covalent bond.[65] Implicitly, the interior of the SWNT would not be as reactive, thus the favourable adsorbtion site for NO_2 would be the exterior of the SWNT, not the interior due to the bonding having covalent character, possibly explaining the lack of IR peak splitting. A combined XPS and theoretical study found that NO_2 adsorption on defective nanotubes is strong and irreversible.[66] Based on these examples of IR shifts, we conclude that the molecules are affected by interactions with SWNTs, creating a unique environment that can alter molecular reactivity.

An interesting study of gas phase adsorption of organic molecules was carried out by Sumanasekera et al.[67] and revealed that π–π interactions are important for adsorption on carbon nanotubes. The authors studied adsorption of a series of structurally related molecules cyclohexane, cyclohexene, cyclohexadiene and benzene (Scheme 1) where the number of
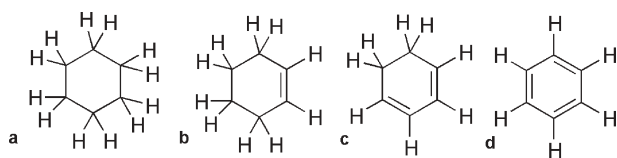
π-electrons monotonically increases from zero to six. The thermopower and resistance of nanotube mats were used to determine the highest adsorption energy for the molecule with the largest π-electronic system (benzene) and the lowest for the molecule without π-electrons (cyclohexane). This result clearly demonstrates that the molecule–NT interactions in this series are controlled by coupling of π-electrons of the molecules with the electronic system of nanotube. This phenomenon becomes very important for interactions of organic molecules with nanotubes in the solution phase, leading to the solubilization of individual nanotubes discussed in the following section.

3.2. Solution phase

Understanding properties of carbon nanotubes in solution and development of their practical applications have been hindered for a long time by their extremely low solubility in all conventional solvents. Chemical groups attached to the nanotube sidewalls can significantly enhance their solubility[22,68] but also create defects, which alter SWNT functional properties. An alternative non-destructive method for nanotube solubilisation is based on non-covalent interactions of ambiphilic molecules (surfactants) with nanotube surfaces: hydrophilic parts of such molecules interact with water and hydrophobic parts are adsorbed onto the nanotube surface (Fig. 5), thus solubilising SWNTs and preventing them from the aggregation into bundles and ropes. The structures of the hydrophilic groups of surfactants are very diverse and their nature defines the efficiency of the dispersion of SWNTs in solution. In the case of charged surfactants such as sodium dodecylsulfate (SDS) or tetraalkylammonium bromide the dispersion of nanotubes is stabilized by electrostatic repulsion between the micelles,[69] and in the case of charge-neutral surfactants, such as polyvinylpyrrolidone (PVP, Scheme 2), mainly due to the large solvation shell created by hydrophilic moieties of surfactants assembled around the nanotube.[70] Hydrophobic parts of surfactants are engaged in direct interactions with the nanotube surface. These interactions can potentially alter properties of nanotubes and, therefore,
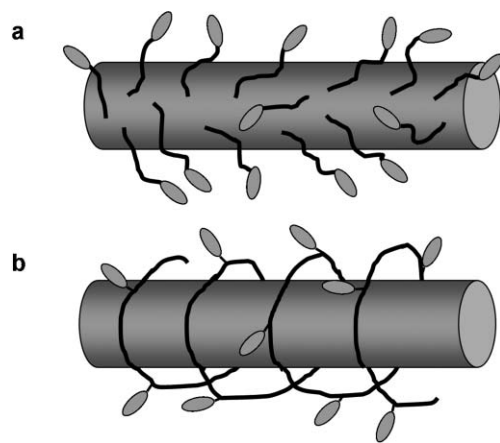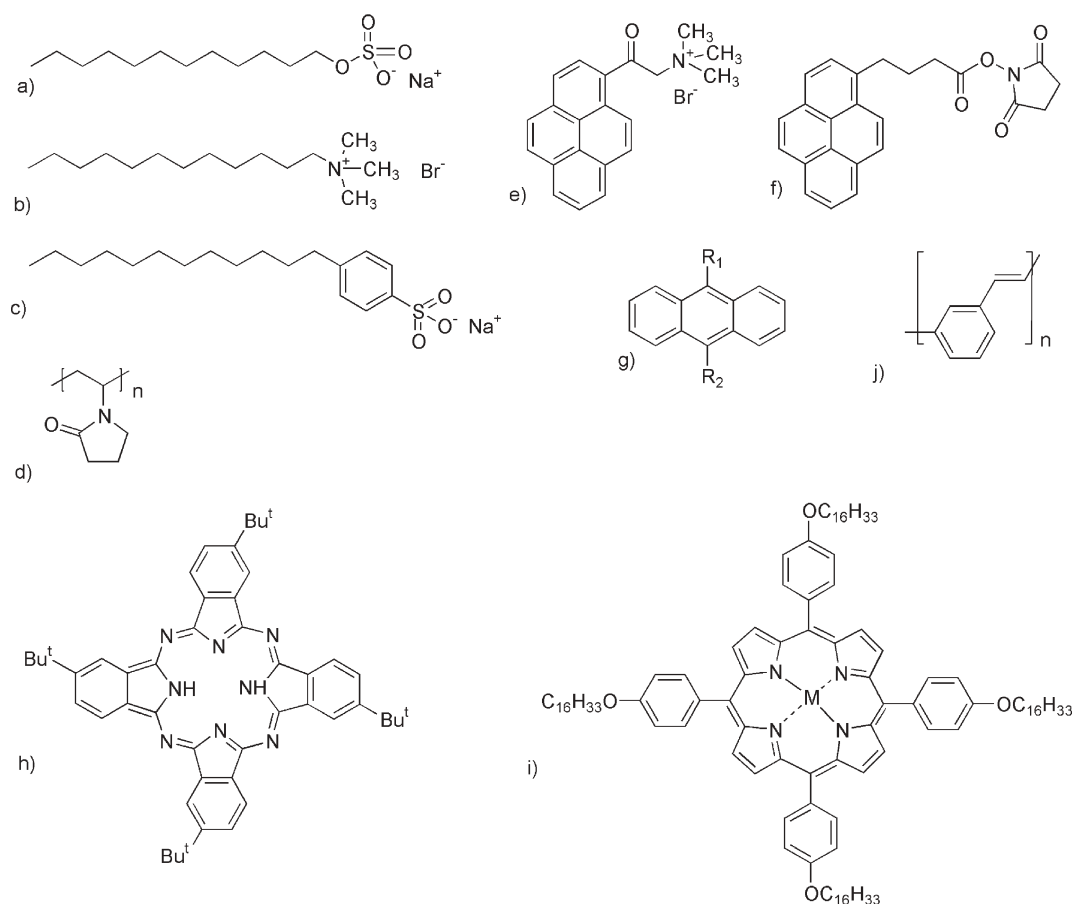

Fig. 5 Different modes of adsorption of ambiphilic molecules on SWNT surface: (a) molecular surfactant forming a micelle and (b) polymer wrapping around nanotube (hydrophilic groups are represented by ellipsoids and hydrophobic groups by black lines).

Scheme 1 Six-member cyclic molecules with different number of π-electrons: (a) cyclohexane, (b) cyclohexene, (c) cyclohexadiene and (d) benzene.

This journal is © The Royal Society of Chemistry 2006

Chem. Soc. Rev., 2006, 35, 637–659 | 643

Scheme 2 Different types of molecules adsorbed on nanotube surfaces for solubilization: (a, c) anionic, (b, e) cationic and (d) polymeric surfactants; (f, g) polyaromatic hydrocarbons; (j) conjugated polymers; (h) phthalocianins, and (i) porphyrins.

are relevant to the topic of this review and discussed in detail for different classes of surfactants.

The anionic surfactant SDS was one of the first molecules whose interactions with nanotubes were thoroughly studied. TEM imaging unambiguously demonstrated that SDS is adsorbed on the surface of MWNTs and arranged into rolled-up half-cylinders with the alkyl-group of each molecule pointed towards the nanotube.[71] It has been shown that such striation patterns formed by molecules on the surface of MWNTs are related to the presence of the long alkyl chains within the structure of the surfactant and are unaffected by the nature of the hydrophilic group. Later attempts of cryo-TEM[70] and HRTEM imaging[72] of SDS micelles on SWNTs revealed no structural organization of this surfactant around single-walled nanotubes, possibly due to their higher curvature than MWNTs. Simple alkyl chains of surfactants such as SDS, sodium dodecyl sulfonate (SDSA), dodecyltrimethylammonium bromide (DTAB) are believed to form non-specific hydrophobic interactions with the nanotubes.[69,70] As a result, the surfactant molecules are only loosely packed around nanotubes and, for example, SDS-SWNT micelles appeared to be relatively unstable as compared to other classes of surfactants such as PVP and surfactin, and the micelles disassociate at low temperatures.[73] The length and the shape of the alkyl chain is very important for the efficiency of the interactions of such surfactants with SWNTs: longer and more

branched alkyl groups are better than linear and straight ones respectively.[74,75] Based on their nanotube solubilising ability, anionic bile salts with cholesterol groups as hydrophobic parts of their structures have been shown to be superior surfactants to other types of molecules possibly because of their ability to form layers that stabilize micelles around the SWNTs.[74]

Surfactant molecules containing aromatic groups are capable of forming more specific and more directional π–π-stacking interactions with the graphitic surface of nanotubes. Interactions of SDS and structurally related sodium dodecylbenzene sulfonate (SDBS) with SWNTs have been compared[75] to demonstrate the role of the aromatic groups. SDS and SDBS have the same length of the alkyl chain but the latter has a phenyl ring attached between the alkyl chain and the hydrophilic group (Scheme 2). The presence of the phenyl ring makes SDBS surfactant more effective for solubilisation of nanotubes than SDS, due to the aromatic stacking formed between the SWNT and phenyl rings of SDBS within the micelle.

Pyrene, a group with a large aromatic system, has demonstrated a very high affinity for the nanotube surface. Derivatives of pyrene can be effectively deposited onto SWNTs in organic solvents with a high surface coverage. In fact, the interaction of the aromatic system of pyrene with nanotube is so effective that functionalized pyrenes have been used for anchoring proteins, small bimolecules[76] and

polymerization catalyst to the nanotubes.[77] Substituted anthracenes are another class of polyaromatic molecules forming specific π–π-interactions with nanotubes. The absorption spectra of anthracenes on SWNTs seem to be unchanged as compared to free molecules in solution, whereas fluorescence emission spectra of the same molecules on SWNTs are red-shifted, indicating a partial electron-transfer from SWNTs onto anthracenes.[78] The adsorption of anthracenes on nanotubes seems to be strong, as the molecules remain adsorbed with extensive washing with organic solvents. However, anthracenes can be replaced by pyrenes, which form stronger interactions with nanotubes.

Heterocyclic polyaromatic molecules such as porphyrins and phthalocyanins also can form effective interactions with nanotubes. Tetrabutyl-substituted phthalocyanin (Scheme 2) adsorbs on nanotubes surfaces forming nano-sized clusters with diameters ranging from several to tens of nanometers which presumably consist of aggregated phthalocyanin molecules.[79] UV-vis absorption peaks of the molecules are broadened and C–H bond vibrations are downshifted as a result of the dispersive interaction with nanotubes. Alkyl-substituted porphyrins (Scheme 2) interacting with SWNTs were shown to improve the dispersability of nanotubes in organic solvents.[80]

It is believed that the nature of the interaction of heterocyclic aromatic molecules with SWNTs is essentially the same van der Waals forces as in the case of polyaromatic compounds such as pyrene. However, the incorporation of a metal ion in the phthalocyanin or porphyrin systems seems to weaken their interactions with the nanotube sidewalls. For example, Zn-complex of porphyrin[80] and Cu-complex of phthalocyanin[79] showed a weaker binding ability to SWNTs as compared to the metal-free molecules. These examples illustrate the importance of the electronic state of the molecule for formation of effective molecule–nanotube interactions.

Ambiphilic polymers are often used for solubilisation of nanotubes. The main advantage of using polymers instead of small molecular surfactants is that the polymers reduce the entropic penalty of micelle formation. Also some conjugated polymers have significantly higher energy of interaction with nanotubes than small molecules with nanotubes. The main problem for polymers is that interactions with mechanically rigid SWNTs may force them into energetically unfavorable conformation. It has been suggested that to minimize strain in their conformations some polymers can wrap around nanotubes in a helical fashion (Fig. 5b).[81] Polyvinylpyrrolidone (PVP), a polymer with a hydrophobic alkyl backbone and hydrophilic pendant groups can be envisaged to coil around the nanotube so that its backbone is in contact with the nanotube surface and pyrrolidone groups are exposed to water.[69,81] Polynucleotides (single-stranded DNA) are arranged in an opposite way to PVP: they have a hydrophilic sugar–phosphate backbone and relatively hydrophobic aromatic nucleotide bases as pendants. A recent study has shown that polynucleotides can form various helical wrappings around the nanotube so that aromatic nucleotide bases are in close contact with the SWNT.[82] Wrapping of polymers based on conjugated poly(m-phenylenevinylene) (PmPV) systems is also very important as it allows formation of very

effective van der Waals interactions between the nanotube and the conjugated backbone. The fact that SWNTs interact with the PmPV backbone rather than its lateral groups has been demonstrated spectroscopically (NMR)[83] and later confirmed by modelling,[84] which also revealed that the permanent dipole moments on the PmPV backbone play an important role for induction of transient dipoles in the NT, providing effective van der Waals interactions with nanotube sidewalls.

4. Endohedral encapsulation of molecules

Typical SWNTs diameters range from 0.7 to 2.0 nm, which enables the encapsulation of a wide variety of molecules in the interior cavity of a nanotube ranging from He^{46} to $Gd_2@C_{92}$.[85] Because of the deep potential well inside the SWNT interior, it is generally very easy to encapsulate molecules, provided the molecules have enough kinetic energy to move to the open ends of SWNTs and overcome the small barrier to entrance at the end.

Dillon *et al.* reported a 5–10% weight uptake of H_2 in bundles of SWNT with open ends, measured with thermal desorption spectroscopy (TDS).[86] This result spurned many researchers to study nanotubes for gas storage. This was one of the first demonstrations of molecular encapsulation in SWNTs, though it was difficult to distinguish between encapsulation of H_2 in SWNTs and adsorption on nanotube surfaces at this stage. The second notable molecule to be observed inside SWNTs was the fullerene C_{60}, directly visualised using high resolution transmission electron microscopy (HRTEM), reported by Smith *et al.* in 1998.[87] The classes of molecules and experimental methods to study them inside nanotubes have been largely defined by these two seminal works. The former class of molecules, small gas molecules and noble gases, on SWNTs has been studied mostly by spectroscopy, notably TDS, BET adsorption, and infrared spectroscopy as described in section 3. The latter class of molecules, thermally stable fullerenes, has been studied mostly by TEM, spectroscopy associated with microscopy, such as electron energy loss spectroscopy (EELS) and energy dispersive X-ray spectroscopy (EDX), and Raman spectroscopy. More recently, there has there been a stronger overlap of the two fields.

4.1. Mechanisms of molecular encapsulation

For molecules in the liquid phase, entry into the interior cavity has a small barrier and is spontaneous if the surface tension of the liquid is below 200 mN m^{-1}.[88,89] Virtually all organic liquids have a surface tension below 200 mN m^{-1}, so insertion will be favourable for most liquid molecular compounds as long as the molecular size is smaller than the nanotube diameter. It is more difficult to provide large molecules with sufficient kinetic energy to free them from the crystal and allow them to diffuse into the SWNT. The implication is that large molecules are generally more firmly trapped inside SWNTs than small molecules, but it is difficult to determine by what means they got there, since more energy is required and thus more possible pathways for encapsulation emerge.

The kinetics of fullerene encapsulation is difficult to determine experimentally due to a lack of distinct spectroscopic
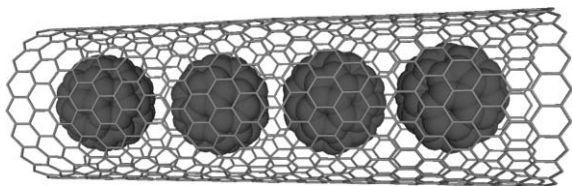
This journal is © The Royal Society of Chemistry 2006

Chem. Soc. Rev., 2006, **35**, 637–659 | 645

Fig. 6 Structural diagram of C_{60}@SWNT.

signatures of encapsulation. Also, theoretical works on the kinetics of fullerene encapsulation are not in agreement.[90–92] Berber *et al.* made the first attempt at studying kinetics of encapsulation of C_{60} in SWNTs.[90] However, their calculated energy of encapsulation, 0.43 eV from gas phase, is almost an order of magnitude lower than other values from a variety of methods.[32,33,93] They found that sidewall defects present the most likely encapsulation route, and that fullerenes have no barrier for encapsulation *via* a sidewall defect. The kinetic energy of a fullerene corresponds to a macroscopic temperature of 400 °C for a successful encapsulation event.[90] Ulbricht *et al.* used a molecular dynamics simulation with experimentally determined Lennard–Jones parameters and found encapsulation at 650 °C to be almost instantaneous,[91] not over several days, as was observed experimentally.[94] They also state that encapsulation is most likely to occur *via* open ends of SWNTs in a bundle with an encapsulation barrier of *ca.* 0.3 eV and an encapsulation energy gain of 3.01 eV.[91] *In-situ* variable temperature HRTEM has shown that fullerenes tend to stick to the outside of nanotubes, then fly into vacuum at approximately 350 °C,[95] with fullerenes spending less time on the SWNTs as temperature is increased. Luzzi and Smith argued that this evidence supported encapsulation *via* surface diffusion, where fullerenes in the gas phase adsorb onto nanotube bundles, then diffuse into openings.

None of these results resolved whether fullerenes can be inserted into nanotubes at or near room temperature which is an important problem for insertion of thermally unstable fullerene derivatives and other molecules into NTs. A study by Berber *et al.* implies that fullerenes or other large molecules would not have enough kinetic energy to enter SWNTs at room temperature, even though there is no barrier for encapsulation.[90] Their observation is based on a relatively narrow window of velocity for fullerenes to enter SWNTs, so thermally 'slow' fullerenes would not have an appropriate trajectory to enter SWNTs. Ulbricht *et al.*[91] imply that encapsulation at sub-650 °C temperatures may be possible, as long as the 0.3 eV barrier can be overcome, which is close to the kinetic energy of a fullerene at room temperature. While high temperature encapsulation works well for fullerenes and endohedral metallofullerenes, it is not appropriate for functionalized fullerenes, some endohedral fullerenes, and a large range of complex organic and bio-molecules that cannot be vaporized without decomposition. Solubilization of such molecules is an effective method to give mobility to large molecules, and filling carbon nanotubes in the solution phase was thought to be an appropriate alternative method to the gas phase filling of carbon nanotubes. In the solution phase we must consider and compare three important parameters: the energy of interaction of fullerene with the NT, the energy of

interaction of fullerene with solvent molecules (*i.e.* solubilisation energy) and the energy of the absorption of solvent into the NT. For example, if the solvent forms very effective interactions with the dissolved fullerene that have a higher energy per fullerene than the energy gain of fullerene encapsulation into NT, then fullerene encapsulation in solution is unlikely to occur. However if solvent interacts with fullerenes and nanotubes only weakly, in principle, the solvent can be used for transporting fullerenes into nanotubes effectively without hindering the encapsulation process.

Several groups have independently developed methods for low-temperature encapsulation of fullerenes in the solution phase that may be applicable to other molecules. The first published work was by Yudasaka *et al.*,[96] where they described two phenomena that allowed encapsulation of C_{60} in SWNTs, called 'nano-extraction' and 'nano-condensation'. Essentially, nano-extraction consists of immersing fullerenes and nanotubes in ethanol to fill SWNTs cavities with C_{60}, and nano-extraction consists of coating nanotubes with a supersaturated fullerene solution in toluene. In this work, the authors used thermally widened nanotubes, such that 50% of the sample contained unusually wide SWNTs greater than 20 nm in diameter. For nanotube filling in ethanol, it was stated that a weak solvent–host and solvent–guest interaction is crucial, and using toluene in the same proportions (10 mL of solvent, 1 mg C_{60}, 1 mg SWNTs) did not lead to fullerene insertion.

Simon *et al.* reported a method for inserting C_{60} and N@C_{60} by refluxing a mixture of these fullerenes with SWNTs in hexane.[97] Once again C_{60} and N@C_{60} are known to have a low solubility in hexane which is indicative of weak solvent–molecule interactions important for successful encapsulation of fullerenes into nanotubes. Although nanotubes filled by this method were extensively characterised by spectroscopy, no TEM evidence for nanotube filling under these conditions was presented. Solvent and gas-phase filled samples showed no difference in filling yield, which is surprising, considering that gas and liquid filling are based on two different mechanisms and occur at very different energy scales. Also, a motivation for the choice and the role of *n*-hexane in filling process or mechanism of encapsulation are not entirely clear.

We found conventional organic solvents to be ineffective at filling SWNTs of internal van der Waals diameters close to that of the van der Waals diameter of C_{60} with fullerenes.[98] In order to rationalise these observations we had to consider that organic solvents dissolving fullerenes can enter into SWNTs as well as fullerenes, which is an important feature of the molecular filling in solution. In a typical fullerene solution, the ratio of dissolved fullerenes to solvent molecules is about $1 : 10^6$, and carbon nanotubes will be predominantly filled with solvent when immersed into a fullerene solution. Therefore, it is important to consider the behaviour of the solvent inside the nanotube as a part of any solution phase filling mechanism. Because desorption of solvent out of SWNT cavities is crucial for the effective filling of nanotubes with fullerenes, geometrical parameters of solvent molecules, such as critical diameter, as well as binding parameters become very important. We found that functionalized fullerenes can be encapsulated inside SWNTs using supercritical CO_2 (scCO_2) without loss of fullerene functionality.[99] The small critical

diameter of CO_2 was important for encapsulating C_{60} in relatively narrow SWNTs. Fullerenes, which have a very low solubility in $scCO_2$, readily enter 1.49 nm diameter SWNTs in a $scCO_2$ medium.[98] However, octasiloxane $H_8Si_8O_{12}$ does not enter nanotubes in $scCO_2$ as efficiently as C_{60} due to the high affinity of octasiloxane for $scCO_2$. Gas phase encapsulation of octasiloxane was found to be substantially more effective, showing that the solvent medium should have a low nanotube affinity and a low guest molecule affinity. After considering the solvent–host and solvent–guest interactions, then critical size of the solvent molecule and appropriate nanotube diameter may be considered.

These works on low temperature nanotube filling bring a suite of techniques for encapsulating molecules in a wide range of nanotubes. It is possible that these methods can be tailored with solvent composition, nanotube diameter, temperature, and pressure to alter guest solubility to insert any given molecule into nanotubes. In most cases, molecules can find their own way into the interior of nanotubes. Often, the most difficult aspect of encapsulating molecules, especially smaller molecules, is keeping them inside the nanotube. Recent work by Matranga and Bockrath[56] shows an effective method to mechanically trap gases inside SWNTs above their desorption temperature. Molecules were trapped inside SWNTs by filling them at low temperature, then exposing the sample to ozone. The nanotube entrance sites reacted with ozone gas and were blocked, hindering the release of endohedrally located CO_2 and SF_6. Molecules adsorbed outside SWNTs were desorbed upon warming the sample, leaving only encapsulated gas molecules. IR signatures of encapsulated molecules remained for at least 24 hours in vacuum and some signal remained even during exposure to air. This result is particularly encouraging for trapping molecules that have low encapsulation energies in SWNTs, and then studying the effect of confining them in nanoscopic volumes. It also could allow small molecules encapsulated in SWNTs to be studied by other techniques, such as transport measurements, photoluminescence, magnetic resonance spectroscopy or EELS.

4.2. Effects of encapsulation on molecules

4.2.1. Transmission electron microscopy: an imaging tool for encapsulated molecules. High resolution transmission electron microscopy enables imaging of materials with atomic resolution. Also this is the only microscopic technique that can see through the sidewalls of nanotubes to visualize their contents. HRTEM can *directly* reveal structural information about molecule packing, can reveal molecular motion in real time, and can show that molecules are genuinely located inside SWNTs, making this technique an invaluable tool for studying molecules within nanotubes. Various molecules have been unambiguously shown to be encapsulated in SWNTs using HRTEM, including fullerenes, endohedral metallofullerenes, *o*-carborane,[100] cobaltacenes,[101] octasiloxane, and pyrelene-3,4,9,10-tetracarboxylic dianhydride (PTCDA).[102] Individual atoms can be imaged for SWNTs filled with ionic salts such as KI[103] or doped with alkali metals such as K.[108] One of the serious disadvantages of TEM techniques is the fact that molecular specimens are significantly affected by the electron

beam during the analysis which can cause ionisation of the molecules and even structural damage. As the techniques for imaging molecules inside nanotubes improve, more direct comparisons between observable structure and positioning of molecules and their spectroscopic signatures can be made.

4.2.2. Molecular ordering inside nanotubes. The arrangement of atoms and molecules plays a substantial role in the bulk properties of a material. By controlling molecular packing and intermolecular interactions it is possible to tune the functional properties of the material. There are several interesting examples of how the phase of molecules changes when inserted into SWNTs studied using HRTEM,[104] diffraction,[45] and theoretical methods.[35] C_{60} fullerenes are a commonly studied example of how confinement in a nanotube can affect molecular phase, since fullerenes are spherical and so analogies to hard sphere packing can be easily drawn. In the bulk crystal, spherical molecules like fullerenes pack in an FCC lattice, with twelve nearest neighbours around each molecule. Fullerenes are surrounded by two nearest neighbours inside a (10,10) SWNT. Theoretically, it was found that C_{60} sits along the central axis of a 1.36 nm (10,10) SWNT.[105] Later works have theoretically[35] and experimentally[104] shown that several phases of fullerenes evolve as the diameter of a nanotube is widened. As the nanotube diameter is increased, C_{60} transitions from a linear phase, to a zig-zag, followed by a double-stranded helix, then a two molecule layer (Fig. 7). Larger diameter nanotubes exhibit a variety of other phases, eventually turning into FCC C_{60} for infinite diameter nanotubes. Spheroidal *o*-carborane molecules also form zig-zag structures in 1.6 nm SWNTs as shown by HRTEM, whereas they crystallise in an FCC lattice in bulk.[100]

Ellipsiodal fullerenes C_{70} show a ''standing'' (long axis of C_{70} perpendicular to the nanotube axis) and ''lying'' (long axis of C_{70} parallel to the nanotube axis) phase for 1.49 nm and 1.36 nm SWNTs, respectively (Fig. 8).[106,107] The type of the
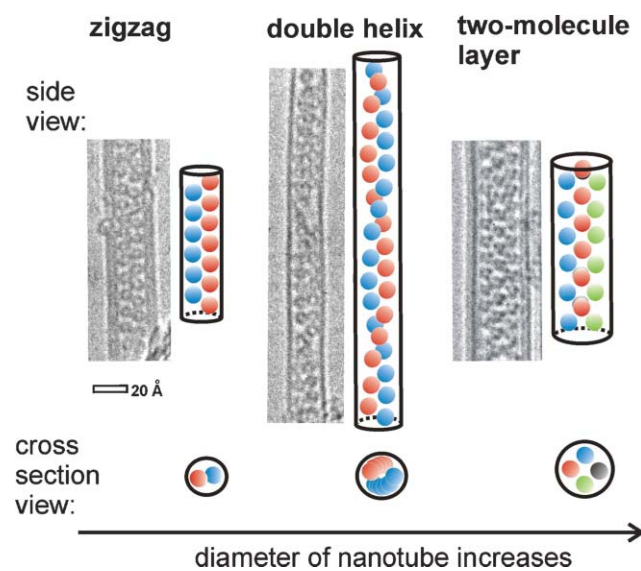

Fig. 7 Different phases of C_{60} assembled in carbon nanotubes of different diameters. (Reproduced with permission from ref. 187, copyright 2005 American Chemical Society.)
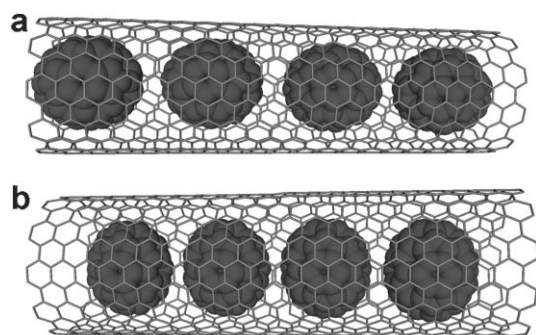
This journal is © The Royal Society of Chemistry 2006

Chem. Soc. Rev., 2006, **35**, 637–659 | 647

Fig. 8 Two orientations of C_{70} observed in SWNTs: (a) longitudinal (C_{70} "lying") orientation in narrower nanotubes and (b) transverse (C_{70} "standing") orientation in wider nanotubes.

orientation of C_{70} is strictly controlled by the diameter of nanotube. As nanotubes widen further, C_{70} and C_{78} are predicted to show new packing phases similar to those of C_{60} inside SWNTs, though the lower symmetry of larger fullerenes compared to C_{60} makes ordering more difficult.[37] New phases of a variety of molecules have been directly imaged inside nanotubes, and more unique phases are expected to be found over time.

The interaction between nanotubes and water is particularly interesting due to the hydrophobicity of graphene structures. H_2O inside SWNTs has been predicted to behave dramatically differently when compared to the bulk, and experiments are beginning to show that unique behaviour. Despite the fact the SWNTs are hydrophobic, molecular dynamics (MD) studies predicted that SWNTs are continuously filled with water when submerged in a bath and exhibit bursts of flow through the SWNT channel.[108] Koga *et al.* predicted that ordered concentric 'ice nanotubes' would form inside SWNTs under pressure,[109] and others predicted that H_2O would form similar tubular structures inside the SWNT cavity at 300 K without external pressure.[110,111] They observed that these ice nanotubes tended to retain some liquid-like properties (*i.e.* molecular mobility), though they show a high degree of ordering, indicating a glass-type solidification behaviour upon cooling. Thus new phases of water were predicted with different transition temperatures and pressures than bulk. The observations of new structural phases of H_2O inside SWNTs was observed using X-ray diffraction by Maniwa *et al.*, where they originally observed heptagonal ice nanotubes,[112] then assigned pentagonal to octagonal ice nanotubes inside different diameter SWNTs.[113] The melting temperature for pentagonal and hexagonal ice nanotubes was found to be greater than for bulk ice, but the melting temperature for heptagonal and octagonal ice nanotubes was lower than bulk ice by greater than 50 K.[113] Using neutron diffraction and inelastic neutron scattering, Kolesnikov *et al.* found that H_2O forms ice nanotubes and also one-dimensional chains of water in the centre of the ice nanotube (Fig. 9).[114] These chains show unusually soft dynamics, maintaining liquid-like behaviour down to 8 K. This dramatic suppression of freezing temperature is attributed to the decreased hydrogen bonding between water molecules in the chain and to a soft, flat potential well in the centre of the ice nanotube.
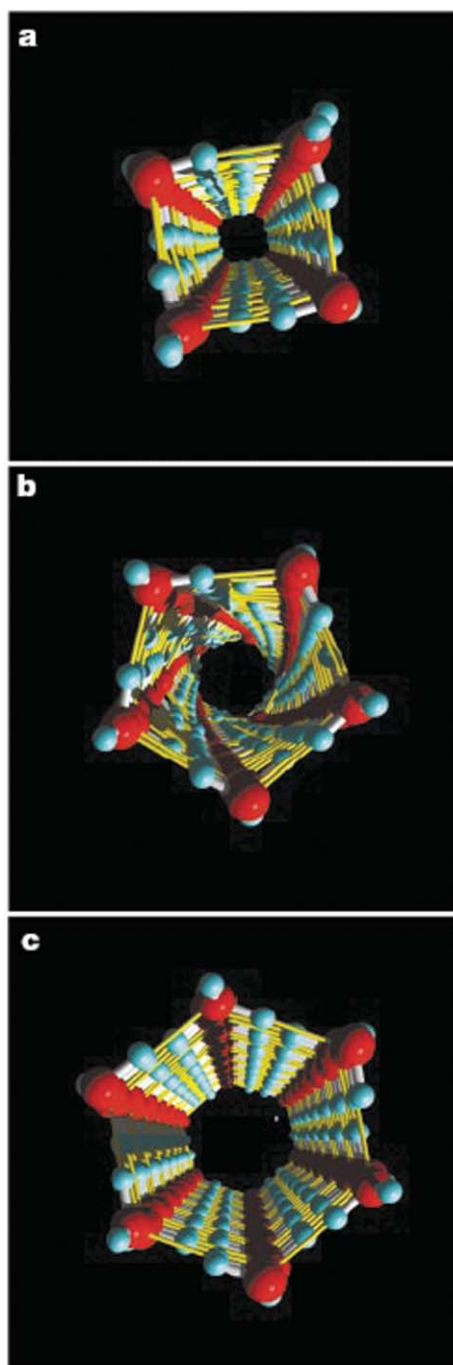

Fig. 9 Snapshots of quenched molecular coordinates: (a) square, (b) pentagonal, (c) hexagonal ice nanotubes in (14,14), (15,15) and (16,16) SWNTs. (Reproduced with permission from ref. 109, copyright 2001 Macmillan Publishers Ltd.)

4.2.3. Molecular dynamics inside SWNTs. Endohedral metallofullerenes containing one or more metal atoms trapped inside a carbon cage can be effectively inserted into SWNTs and present an opportunity for studying the dynamics of molecular rotation inside a nanotube, due to the high single-atom contrast of metal atoms in HRTEM. The atoms inside bismetallofullerenes can exhibit tumbling motion ($La_2@C_{80}$),[115] total immobility ($Sc_2@C_{84}$),[116] or thermal oscillations ($Gd_2@C_{92}$)[85] inside nanotubes. The motion of
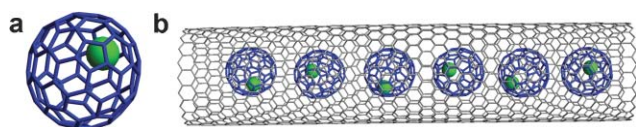
Fig. 10 Structural diagram of (a) endohedral metallofullerene $M@C_{82}$ and (b) $(M@C_{82})@SWNT$ peapod structure.

two La-atoms in $(La_2@C_{80})@SWNTs$ was compared to NMR experiments of $La_2@C_{80}$ in solution.[115] While the La_2 cluster in solution showed free rotation at room temperature, the La_2 cluster in $(La_2@C_{80})@SWNT$ peapod showed a 'ratcheting' behaviour, which was ascribed to charge transfer from the fullerene to the nanotube. $Ce@C_{82}$ also shows unique dynamic behaviour in isolated SWNTs and in bundles.[117] $Ce@C_{82}$ showed a saltatory molecular rotation in an isolated $(Ce@C_{82})@SWNT$, where the molecule was observed to hop to different orientations over time. In a bundle of $(Ce@C_{82})@SWNTs$ the rotation appears to be faster as the cerium atom of $Ce@C_{82}$ was visualised as several dark dots on HRTEM micrographs. This behaviour was qualitatively different from that reported for $Ce@C_{82}$ in the crystal. Since endohedral metallofullerenes possess high dipole moments and the intermolecular dipole–dipole interactions scale as the inverse of distance between the molecules cubed, bundles of $(M@C_n)@SWNTs$ behave as highly anisotropic three dimensional structures, rather than as one-dimensional crystals.[94] Since the energy of dispersive interactions scales with the inverse of distance to the sixth power, all-carbon peapods $C_n@SWNTs$ may still be considered one-dimensional crystals, since fullerene–fullerene interactions in adjacent nanotubes will be small compared to nearest neighbour interactions.

4.2.4. Chemical reactions inside SWNTs. There is growing work on the effect that SWNTs have on reactions of molecules inside nanotubes. One notable work by Halls and Schlegel[185] reported calculations for the Menshutkin S_N2 reaction inside SWNTs and in the gas phase. They found that the activation energy and reaction endothermicity were substantially reduced inside the SWNT due to the highly polarisable nanotube wall. They note that the reaction inside a SWNT resembles that of reaction in low-dielectric (generally nonpolar) solvents. Very recently, Halls and Raghavachari[118] calculated that the energy barrier for the Cl^- exchange S_N2 reaction inside a SWNT had an increased barrier compared to the gas phase by 6.6 kcal mol^{-1} (286 meV). When these results are taken with the results from the Menshutkin S_N2 reaction, the interior of a nanotube can be considered a solid solvation environment.[118] These theoretical results have not been directly paired with experiments, but recently there has been progress on experimental evidence of reactions inside SWNTs.

Using the fact that SWNTs are thermally very stable, reactions between molecules inside SWNTs can be initiated by heat. Bandow *et al.* have shown that fullerene C_{60} reacts inside nanotubes to form a concentric SWNT inside the host SWNT at temperatures about 900 °C.[119] Also, Fujita *et al.* found that PTCDA (Scheme 3b), which normally forms a 2D graphene sheet at 2,800 °C, transformed into a nanotube templated by a host SWNT at 1050 °C, indicating a *substantially* lower barrier
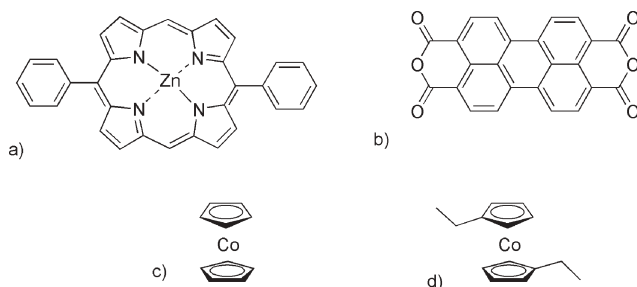
Scheme 3 Non-fullerene molecular compounds encapsulated in SWNTs: (a) phenylporphyrine, (b) PTCDA, (c) cobaltocene and (d) ethyl cobaltocene.

for transformation inside a SWNT.[102] At lower reaction temperatures more suitable for typical organic transformations, we have found that nanotubes can template polymerisation of $C_{60}O$ to form $(C_{60}O)_n$ inside SWNTs, giving a linear, unbranched product (Fig. 11).[120] Pichler *et al.*[121] studied the evolution of $C_{60}@SWNT$ doped with potassium vapour using *in-situ* Raman. They found that the fully doped $C_{60}@SWNT$ behaved as a metal and exhibited many of the Raman signatures of o-RbC_{60} polymer and Rb_6C_{60}. Based on Raman measurements, they found that the fullerenes formed a $(C_{60}{}^{6-})_n$ polymer inside the SWNT, another example of a chemical transformation inside SWNTs. They assigned this structure based on the known relation of a downshift of the $A_g(2)$ Raman mode of C_{60} for both charge transfer and covalent bond formation. This interesting chemical reaction can be initiated inside SWNTs *via* electron transfer from external alkali metals to SWNT. Liu *et al.* observed a shortening of the interfullerene spacing in SWNT upon potassium doping from 0.99 nm to 0.96 nm using electron diffraction.[122] HRTEM images by Guan *et al.*[186] show that potassium doped peapods $C_{60}@SWNTs$ have some K atoms inside the SWNT, and that the only way to achieve full doping of C_{60} would be from electrons transferred to the fullerene *via* the SWNT.

Some chemical transformations take place spontaneously upon insertion of molecules into nanotubes. It was shown that iodine molecules I_2 enter SWNTs and form double helices in
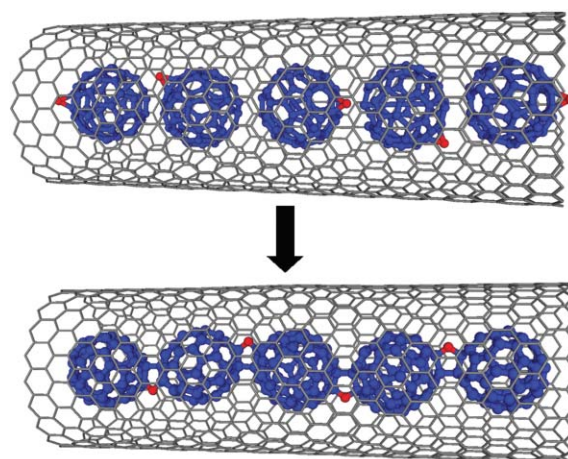

Fig. 11 Polymerisation of $C_{60}O$ inside carbon nanotube.

This journal is © The Royal Society of Chemistry 2006

Chem. Soc. Rev., 2006, **35**, 637–659 | 649

SWNTs of appropriate diameter.[123] Iodine exists as the neutral molecule I_2 in crystalline form and in the gas phase. In the molten state, iodine exists as iodinium (I^+) and polyiodide (I_3^-) species. However, the iodine inside SWNTs converts to I_3^- and I_5^-, with no observable I_2, based on Raman and XPS data.[124] When SWNTs are completely filled with iodine, all iodine converts to I_5^-, seen by a prominent peak at 175 cm^{-1} in Raman spectra. *Ab-initio* calculations of iodine chains of three and five atoms adsorbed on a curved graphitic sheet found that the chains prefer to be straight, whereas three neutral iodine atoms in vacuum prefer a bent arrangement.

Nitric oxide NO has been absorbed into SWNTs and studied with IR spectroscopy by Byl *et al.*[55] It was found that only the *cis*-$(NO)_2$ dimer was observed to be adsorbed on the interior of SWNTs. In the gas phase, 99% of NO exists as a monomer, and in the condensed phase, a number of isomers of $(NO)_2$ exist, though *cis*-$(NO)_2$ is the most stable structure. The authors found large downshifts of the stretching modes of $(NO)_2$ and also determined an energy to remove the $(NO)_2$ signal through thermal desorption equal to 157 meV. This energy is greater than or equal to the energy to break the N–N bond of the dimer, supporting their assignment of the $(NO)_2$ dimer, rather than the NO monomer. Their observation was in contrast to calculations by Turner *et al.*, who reported that 70% of NO in SWNTs would be monomeric[125] under the experimental conditions of Byl *et al.* Zhao *et al.* found that $(NO)_2$ is stabilized relative to the monomer by interacting with an aromatic system. The relative stability of the dimer is due to charge transfer from the aromatic ring to the NO. Nitric oxide is a more reactive species as a dimer, therefore $(NO)_2$ adsorbed on SWNTs could be used to initiate novel reactions.[126] Though there is little work so far on reactions in SWNTs, it is clear that SWNTs can both serve as a new reaction environment and template reaction products.

5. The effect of molecules on nanotube properties

Just as SWNTs can alter molecular behaviour, molecules can alter nanotube mechanical and electronic properties. An encapsulated molecule in principle can affect the nanotube through dispersive interactions, charge-transfer, or mechanical strain. Each of these effects should have unique spectroscopic signatures manifested in changes in nanotube structure and in its electronic properties. Three main spectroscopic methods are conventionally used for studying the effect of molecules on nanotubes as illustrated in the following sections: Raman, absorption, and photoluminescence spectroscopy.

5.1. Raman spectroscopy

Raman spectroscopy is particularly useful in characterising SWNTs, since it gives information about the physical structure and electronic properties of SWNTs.[127] A typical Raman spectrum has a radial breathing mode (RBM) region between 100–500 cm^{-1}, and the RBM frequency is inversely proportional to the SWNT diameter. Because Raman is a resonant process, not all SWNT diameters are excited equally by excitation at a given wavelength, and a range of laser excitations must be used to determine a realistic diameter distribution of the sample. Also, changes in SWNT properties
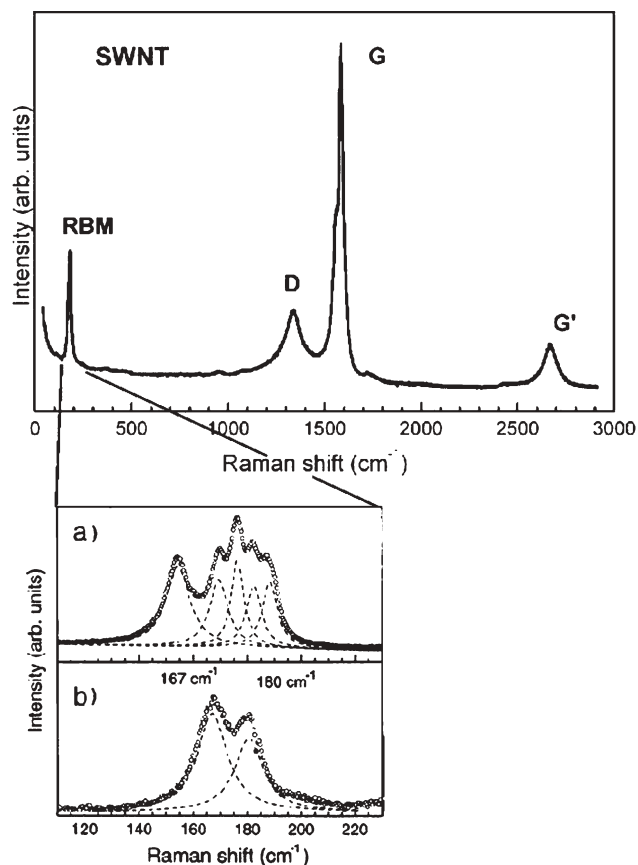

Fig. 12 Typical Raman spectrum of SWNTs (inset: magnified RBM area illustrating several peaks corresponding to nanotubes of different diameters. (Courtesy of S. Lyapin.)

induced by molecules can affect the RBM resonance conditions. Thus RBM peaks can appear to shift when one specific chirality SWNT is falling out of resonance and another one is coming into resonance. Also, the graphitic in-plane stretching G mode is an important feature of SWNTs Raman spectra in the *ca.* 1580 cm^{-1} region.

Bandow *et al.* observed that fullerenes inserted into SWNTs caused a downshift in the RBM of nanotubes wider than 13.7 Å.[128] A downshift in RBM is explained by softening of the C–C bonds of the SWNT sidewall, corresponding to exothermic fullerene encapsulation. Shifts in other Raman peaks were not observed when fullerenes were inserted into nanotubes, largely because the RBM is considered especially sensitive to changes in the electronic structure of bonds of the nanotube. A large body of evidence supports an exclusively dispersive (*i.e.* van der Waals) interaction between all-carbon fullerenes and nanotubes,[19,32,33,91,106,129,130] which cause a downshift in RBM of SWNTs of the order 3 cm^{-1}.[106,128]

Transfer of charge to and from SWNTs can alter C–C bonds in the nanotube and thus the SWNT's electronic properties. There is theoretical evidence that semiconducting SWNTs are intrinsically p-doped due to curvature of the graphene sheet.[24] One of the most direct ways to observe the effect of charge transfer is to dope SWNTs with strong electron acceptors or donors, such as halogens or alkali metals, respectively. Removing a small amount electronic density from SWNTs

Table 2 Effect of encapsulated molecules on RBM Raman modes of SWNTs (RBM shift caused by encapsulation is shown in square brackets)

Dopant	RBM position [shift]/cm^{-1}	Dominant interaction
C_{60}[128]	140 [−1], 146 [−1], 160[−2], 170 [−3], 179 [−3,+2]	dispersion
C_{70}[106]	167 [−3], 180 [−2]	dispersion
C_{76}[128]	140 [−1], 146 [−1], 160[−1], 170 [−2, +3], 179 [0]	dispersion
C_{78}[128]	140 [−1], 146 [−1], 160[−2], 170 [−2, +3], 179 [0]	dispersion
C_{84}[128]	140 [−1], 146 [−1], 160[−1, +3], 170 [0], 179 [0]	dispersion
$Ce@C_{82}$[117]	167 [−4], 180 [−3]	dispersion
$CoCp_2$[101]	248 [0]	electron donation, dispersion
Zn-diphenyl porphyrin[150]	165 [+5], 181 [+3]	electron donation, dispersion
Cs[132]	~200 [+2.5]	electron donation
PTCDA[102]	161 [+20], 179 [+3]	electron withdrawal, dispersion
Iodine[131]	192 [+4], 219 [+2], 258 [+1], 284 [0]	electron withdrawal
H_2SO_3[131]	192 [+9], 219 [+6], 258 [+3], 284 [+3]	electron withdrawal
$SOCl_2$[131]	192 [+17], 219 [+7], 284 [+6]	electron withdrawal

with $SOCl_2$ or iodine, for example, causes an upshift in RBM of 4–8 cm^{-1}, which indicates a stiffening of C–C bonds upon doping.[131] Chen *et al.* recently observed that light doping of SWNTs with caesium, which adds a small amount of electronic density to the nanotube bonding orbitals, results in upshifts of RBM modes of *ca.* 2.5 cm,$^{-1}$ [132] which is understood as an increase in energy and hardening of the C–C bond. Further alkali metal doping of SWNTs causes the suppression of RBMs and a downshift of the G mode.[133] This downshift is explained by weakening the C–C bonds and changing the resonance conditions at a given laser wavelength, which can cause the suppression of some peaks, including RBM. It is surprising that the same direction of RBM shift is seen for addition and removal of small amounts electronic density,[132] making RBM shifts as a measure of charge transfer ambiguous without prior knowledge of the molecule's electron affinity or ionisation potential.

It has been suggested that strain imparted by molecules inside SWNTs also can cause significant changes in nanotube bonds. However, it is not clear how strain would affect the relevant Raman modes of SWNTs. Strain can be tensile or compressive, but the difference of tension and compression does not necessarily mean that each will have spectroscopic shifts in different directions. Raman studies of nanotubes under hydrostatic pressure have shown that Raman modes,[134,135] and specifically RBMs,[136] *upshift*, corresponding to a shortening or stiffening of C–C bonds. Also, solvents exert a 'pressure' on molecules due to strong solvation. Bundles of nanotubes have been directly compared in solvent and in vacuum, showing that the D′-mode Raman peak upshifts with increasing solvent cohesive energy density, which is a measure of pressure induced by different solvent environments.[137,138] There are fewer studies of the effect of tensile strain on nanotube Raman modes. Cronin *et al.* showed that individual nanotubes under tensile strain exhibit a *downshift* in G′, G and D modes. The original positions of the peaks were restored upon breaking of the nanotube, which confirms that the observed behaviour was elastic.[139] The authors do not observe a change in RBM with tensile strain for semiconducting SWNTs, but note that the percentage shift of other peaks would result in RBM shifts of less than 2 cm^{-1}, which was within experimental uncertainty.[139,140] They also calculated that strain affects the resonance condition of RBMs, which would result in changing the intensity of the RBM with strain.[140]

A molecule inside a nanotube can only cause tensile strain in the SWNT sidewall, if any strain at all,[141] which should be observed as a downshift in RBM, based on the work described above. Bandow *et al.* filled nanotubes with different fullerenes and observed an upshift of RBM peaks corresponding to small-diameter SWNTs by *ca.* 2 cm^{-1}. For C$_{60}$@SWNT the 179 cm^{-1} SWNT RBM peak (d = 1.37 nm) splits into a 176 cm^{-1} and 181 cm^{-1} peak. The authors attributed the upshift to strain in the SWNT sidewall due to a tight-fit encapsulation. This observation clearly contrasts with the trend that tensile strain causes downshifts in Raman modes. The apparent upshift could be due to a change in resonance conditions of smaller SWNTs, causing an enhancement in the particular peak, or possibly to charge transfer between fullerenes and SWNT.

Endohedral metallofullerenes M@C_n tend to differ from empty-cage fullerenes in that they have smaller HOMO-LUMO gaps, with a higher electron affinity than corresponding empty-cage fullerenes.[142] It has been suggested that there is a substantial charge transfer and strain in nanotube sidewalls produced by metallofullerenes using a variety of local probe techniques and theoretical calculations.[143–146] We would expect to see significant changes in Raman spectra of metallofullerene filled nanotubes as a result of such electronic and structural changes in SWNTs. We have inserted Ce@C$_{82}$ into SWNTs of 1.49 nm and 1.36 nm in diameter with a filling rate of ~70%.[117] We observe downshifts of both RBM peaks of *ca.* 4 cm^{-1}. All other Raman peaks remain in the same position. Such a molecule is larger and should have a greater dispersive interaction with SWNTs sidewalls than C$_{60}$ or C$_{70}$. Debarre *et al.* saw dramatic changes in the Raman spectrum of (La$_2$@C$_{80}$)@SWNT and attributed a 6 cm^{-1} shift in G band to charge transfer.[147] However, the authors did not directly take into account the potentially damaging effects of the excitation laser,[148] making spectroscopic data difficult to interpret and to connect back to a known physical system.[149] We did not observe such dramatically different behaviour for monometallofullerene peapods (M@C$_{82}$)@SWNTs compared to pristine SWNTs. Our observation of a 4 cm^{-1} downshift in RBM indicates that either dispersive interactions, similar to those for C$_{60}$ and C$_{70}$, dominate metallofullerene–nanotube interactions or that several types of interactions cancel each others' shift.

The picture is also murky for polyaromatic organic molecules inside SWNTs. The insertion of Zn-diphenyl

This journal is © The Royal Society of Chemistry 2006

Chem. Soc. Rev., 2006, **35**, 637–659 | 651

porphyrin into SWNTs caused an RBM upshift of 3–5 cm^{-1}, which was attributed to sidewall strain.[150] Metalloporphyrins are considered good electron donors[151] that can give electrons to SWNTs,[152–154] which would cause the characteristic upshift of RBMs associated with addition of electronic density seen for Cs doping.

A very recent study of PTCDA, an electron deficient polyaromatic molecule,[155] encapsulated inside SWNTs showed a 20 cm^{-1} upshift in RBM for 1.54 nm SWNTs and a 3 cm^{-1} upshift for 1.38 nm SWNTs.[102] The magnitude of the shift was ascribed to greater mechanical strain in wider SWNTs due to more molecules encapsulated. Yoon et $al.$ showed that narrow SWNTs filled with fullerenes have more tensile sidewall strain than wide SWNTs,[141] which would lend to an alternative explanation for the observed RBM shifts for PTCDA@SWNTs. Intuitively, PTCDA covering an infinite diameter SWNT ($i.e.$ planar graphite) would not impart any strain on the C–C bonds of the graphene sheet, but PTCDA filling an exceptionally narrow SWNT would impart a large strain on the C–C bonds of the nanotube. However, the observation of an RBM upshift agrees with the PTCDA acting as an electron acceptor, similar to the upshift in RBM that was seen for adsorption of iodine and SOCl$_2$ onto SWNTs.[131] Wider SWNTs doped with SOCl$_2$ show a greater RBM shift than narrow SWNTs,[131] in agreement with the behaviour of PTCDA inside SWNTs.[102]

SWNTs filled with cobaltacene and ethyl cobaltacene were shown to dope SWNTs with electrons at or above a critical diameter required for encapsulation of these molecules, as shown by a shift of photoluminescence peaks of SWNTs and a change from CoCp$_2$ to CoCp$_2^+$ upon encapsulation.[101] However, no shifts in RBMs were seen, possibly indicating that an upshift due to charge transfer interactions was cancelled by a downshift from dispersive interactions.

There is no evidence for any charge transfer between the conjugated polymer PmPV and nanotubes, but van der Waals interactions in SWNT–PmPV complexes are very efficient, exceeding the efficiency of similar interactions between neighbouring nanotubes within a bundle.[156] As a result the RBM Raman peaks of nanotubes interacting with PmVP are up shifted by +7 cm^{-1} more than for nanotubes aggregated in bundles. The polymer-induced direction and magnitude of RBM shifts are similar to hydrostatic compressive strain effects discussed earlier.

### 5.2. Absorption spectroscopy

Single-walled carbon nanotubes exhibit a well-defined absorption features in the near-IR (NIR) range corresponding to the electronic transitions between valence and conduction bands. SWNTs have three electronic transitions in the NIR region: the first semiconducting transition (S$_{11}$) at $ca.$ 0.7 eV, the second semiconducting (S$_{22}$) transition at $ca.$ 1.2 eV, and the metallic transition (M$_{11}$) at $ca.$ 1.8 eV. Optical absorption measurements provide valuable information about electronic properties of semiconducting SWNTs such as band-gap (the S$_{11}$ value), and they also can be used to study interaction of molecules with nanotubes. Species with large electron affinities or small ionisation potentials can withdraw or donate electrons

from/to SWNTs, respectively, which affect the intensity of the absorption peaks. It is interesting to note that electron donors (K, Cs) or electron acceptors (I$_2$, Br$_2$) show very similar changes in the near-IR spectra of nanotubes suppressing the electronic transitions as a result of filling/depletion of the nanotube bands with electrons.[157]

Molecular dopants that cause charge transfer also affect NIR transitions, causing suppression upon increase of doping. Petit et $al.$ showed that lithium–organic molecule solutions with different redox potentials caused suppression of NIR peaks to varying degrees.[158] The mechanism of doping was ascribed to the radical anion of the organic molecule donating electrons to the SWNTs. A thin film of SWNTs was exposed to a lithium–naphthalene complex (redox potential = 2.5 eV) in THF, and all the NIR transitions were suppressed, indicating that electrons fully filled the empty states of semiconducting and the metallic nanotubes. Lithium–fluorenone (redox potential = 1.3 eV) doping cause full suppression of the S$_{11}$ transition and partial suppression of the low energy portion of the S$_{22}$ peak, leaving the M$_{11}$ peak unaffected. Lithium–anthraquinone (redox potential = 0.85 eV) doping caused full suppression of the S$_{11}$ transition, but the other two transitions were not affected. In a later paper, the same group correlated the dopant redox potential with charge carrier density.[159] An increase in charge carrier density and redox potential caused an increase in SWNT film conductivity, showing that charge transfer was responsible for doping. The doping changes were found to be reversible by exposure to molecules with appropriate redox potentials.

Takenobu et $al.$ found that by insertion of organic molecules with suitable electron affinity and ionisation potential into SWNTs it is possible to control selectively the type of the nanotube doping to be p- or n-type.[160] The authors observed a decrease in optical absorption around 0.68 eV, similar to that for SWNTs doped with alkali metals and halogens. To further support their assignment of doping due to molecule encapsulation, they studied their filled SWNTs with other methods. The molecules also induce dramatic changes in Raman spectra of SWNTs including significant reduction of RBM intensity for a strong electron acceptor tetracyanoquinodimethane (TCNQ) and a strong electron donor tetrakis(dimethylamino)ethylene (TDAE) inserted in SWNTs (Scheme 4); a similar behaviour was observed for heavily potassium doped SWNTs.[133] The observed charge transfer between encapsulated molecules and nanotubes was confirmed theoretically,[161,162] and further work on TCNQ@SWNTs using XPS and NEXAFS showed that the SWNTs had donated electrons to the TCNQ.[163]

Recently, Skákalová et $al.$ studied the effect of the interaction of a range of electron donating and electron accepting molecules with SWNTs and showed that all types of molecules cause a decrease of the S$_{11}$ and S$_{22}$ interband
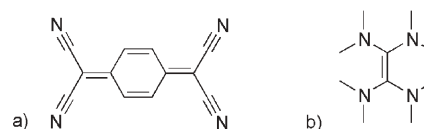
Scheme 4 (a) Strong electron acceptor TCNQ and (b) strong electron donor TDAE inserted into SWNTs.
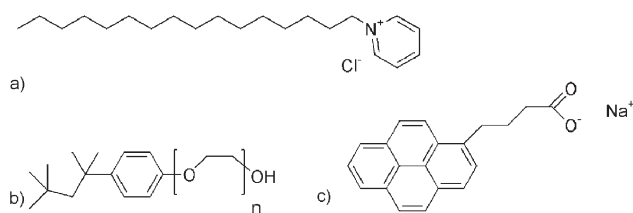
Scheme 5 Structures of surfactants used for PL studies of nanotube dispersions in water (a) CPCl, (b) Triton X-100 and (c) SPB.

transitions in NIR absorbance spectra for semiconducting tubes regardless the nature of the molecules. However, SWNTs absorbance in the far infrared (FIR) region appears to correlate well with electrical conductivity of nanotube mats due the presence of free carriers in nanotube bands, which is proportional to the number of charge carriers introduced by the molecules.[131] Specifically, electron acceptors cause an increase in FIR absorbance and electrical conductivity, whereas electron donors cause a decrease in both measures.

The effect of the molecular doping of nanotubes caused by adsorbed or encapsulated molecules is not dissimilar to electrochemical doping demonstrated for thin films of SWNTs and fullerene-filled SWNTs deposited on an ITO electrode.[164] Nanotube and peapod optical absorption spectra measured as a function of the electro-chemical potential showed suppression of the nanotube absorption bands which appear to be similar for empty SWNTs and $C_{60}@SWNT$ or $C_{70}@SWNT$, indicating a weak coupling between the electronic bands of nanotubes and the orbitals of encapsulated fullerenes.

The interaction of hydrogen ions with SWNTs suspended in aqueous media has been studied spectroscopically by Strano *et al.* showing that protons adsorb on nanotube sidewalls, localising valence electrons and thus suppressing the optical absorption intensity for transitions corresponding to the 1st van Hove singularities.[165] By measuring the changes in the optical spectra of SWNTs as a function of proton concentration the authors found the proton adsorption is a bandgap selective process: metallic nanotubes are protonated first, followed by successive protonation of semiconducting nanotubes with increasing bandgap as the concentration of H^+ increases. Li *et al.* developed this idea further using potassium hexacyanoferrate(III) $K_3[Fe(CN)_6]$ as an oxidant for nanotubes in aqueous solutions.[166] Hexacyanoferrate also exhibits bandgap selective interactions with nanotubes, preferentially doping SWNTs with narrower bandgaps. The oxidation potential of $K_3[Fe(CN)_6]$ can be conveniently controlled by pH of the solution, which enables selective and reversible p-doping of SWNTs in the solution phase.

It should be noted that covalent additions to the SWNT sidewall also causes suppression of NIR transitions,[21,167] so demonstrating SWNT charge transfer requires using techniques in conjunction with NIR, such as film conductivity, FIR absorbance, or monitoring the oxidation state of the dopant molecule. For example, Li *et al.* used UV-Vis spectroscopy to show that $Co(Cp)_2$ and $Co(CpEt)_2$ converted to positively charged ions upon insertion into SWNTs, which confirmed charge transfer effects observed in NIR and photoluminescence spectroscopy.

5.3. Photoluminescence spectroscopy

Optical excitation of nanotubes promotes their valence electrons to higher energetic levels followed by rapid electronic relaxation before emission of a photon with energy corresponding to the nanotube bandgap, which forms a basis for photoluminescence spectroscopy (PL) widely used for characterization of nanotubes. Solubilization of nanotubes in SDS micelles enabled recording the photoluminescence spectra of semiconducting SWNTs in the liquid phase.[69] Since then PL spectroscopy has been an invaluable tool for measuring the effect of surfactants and other molecules adsorbed on the SWNTs surfaces on the electronic structure of nanotubes. A recent comparative study on a large number of different surfactants on SWNTs demonstrates that Raman spectral profiles and the positions of RBM and G-mode peaks are not affected by the nature of the surfactant, whereas the interband electronic transitions in PL are very sensitive to the surfactant (Table 3).[70] For molecules with simple alkyl hydrophobic chains such as SDS the same study revealed a clear linear correlation of the spectral shift of PL peaks with the fluorescent yield: the greater the shift, the smaller the fluorescent yield.

The aromatic pyridinium ring in cetylpyridinium chloride (CPCl) interacting with the nanotube by a π–π-stacking mechanism causes a downshift of PL peaks by 200 cm^{-1} observed for this surfactant, compared to SDS.[74] Surprisingly the same study reports no spectral shifts, relative to SDS, for other surfactants containing phenyl rings including SDBS and Triton X-100 and an upshift of 100 cm^{-1} recorded for sodium pyrenebutyrate (SPB) incorporating a larger pyrene aromatic

Table 3 Shifts of PL peaks of SWNTs induced by interactions with different molecules

SWNT treatment comparison	PL shift, relative to SDS/cm^{-1}	Type of molecule
in vacuo[168]	+225	none
SPB[74]	+100	anionic surfactant
CPCl[74]	−220	cationic surfactant
Cholate[169]	−100	anionic surfactant
SDBS[70]	+2	anionic surfactant
SDSA[70]	−30	anionic surfactant
Sarkosyl[70]	−117	anionic surfactant
TREM[70]	−47	anionic surfactant
PSS-70[70]	−214	anionic surfactant
DTAB[70]	−129	cationic surfactant
CTAB[70]	−124	cationic surfactant
Brij 78[70]	−203	nonionic surfactant
Brij 700[70]	−106	nonionic surfactant
Tween 85[70]	−79	nonionic surfactant
Triton X-405[70]	−119	nonionic surfactant
PVP-1300[70]	−211	nonionic polymer
EBE[70]	−75	nonionic polymer
Pluronic P 103[70]	−68	nonionic polymer
Pluronic P 104[70]	−69	nonionic polymer
Pluronic P 105[70]	−70	nonionic polymer
Pluronic F 108[70]	−95	nonionic polymer
Pluronic F 98[70]	−97	nonionic polymer
Pluronic F 68[70]	−103	nonionic polymer
Pluronic F 127[70]	−84	nonionic polymer
Pluronic F 87[70]	−105	nonionic polymer
Pluronic F 77[70]	−208	nonionic polymer
SDS with CoCp$_2$ filling[101]	−158	anionic surfactant/redox active metallocene

This journal is © The Royal Society of Chemistry 2006

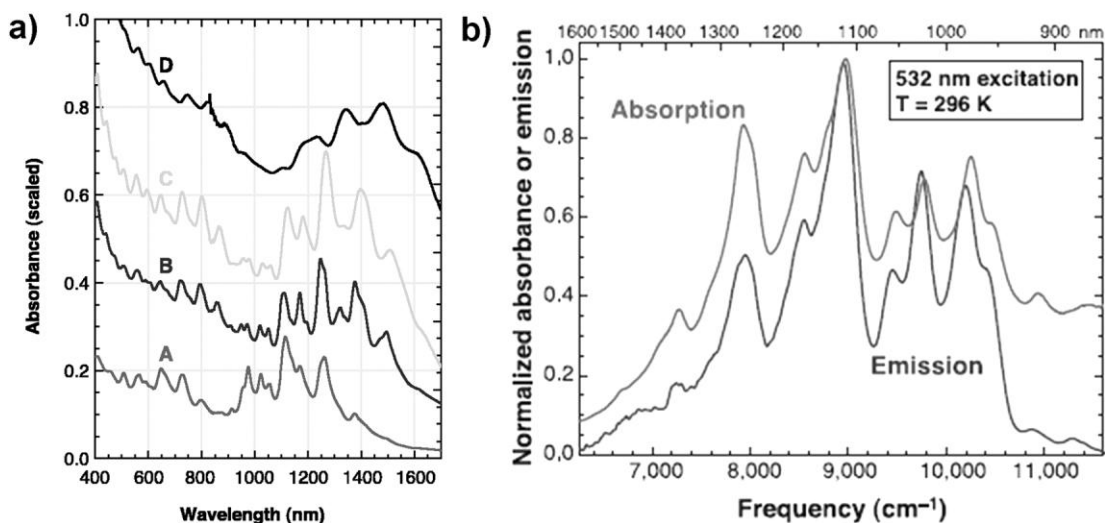*Chem. Soc. Rev.*, 2006, **35**, 637–659 | 653

Fig. 13 (a) Near-IR absorption spectra of carbon nanotubes in SDS-D_2O suspension: individual nanotubes separated and solubilized by SDS micelles (traces A and B); SDS micelles of individual nanotubes after addition of PVP (trace C); nanotubes aggregated in small bundles (trace D). (b) PL emission spectrum of individual nanotubes suspended in SDS micelles in D_2O excited by 8 ns, 532 nm laser pulses, overlaid with the absorption spectrum of the sample in this region of first van Hove band gap transitions. (Reproduced with permission from ref. 69, copyright 2002 AAAS.)

group, which is well-known to form strong interactions with nanotubes. These observations indicate that the simple presence of an aromatic group within the surfactant is not sufficient for formation of π–π-stacking with nanotubes and that steric accessibility of these groups as well as their electronic structure are important for this type of interaction.

Most of polymers adsorbed on nanotubes cause a downshift of PL peaks in rage of 70 to 200 cm^{-1},[70] which indicates that the polymers wrapped around SWNTs create a more polarisable environment resulting in changes in exciton binding energies manifested in spectral shifts in PL.[69,73]

Redox active molecules of cobaltocene encapsulated inside SWNTs have a pronounced effect on the PL spectra of nanotubes.[101] The photoluminescence emission peaks of the SWNTs hosting the molecules are downshifted by 80–220 cm^{-1} with respect to unfilled nanotubes, whereas RBM peaks in Raman spectra of filled nanotubes remain unchanged, as discussed earlier. Systematic spectroscopic studies of CoCp$_2$@SWNT combined with HRTEM imaging revealed a complex mechanism of the interaction of cobaltocene with the nanotube interior: the guest-molecule effectively transfers one electron onto the nanotube electronic bands, and the positively charged cobaltacenium cation resides inside the SWNT without exerting any elastic strain, which causes the shift in PL emission but does not change the RBM spectrum of filled SWNTs.

5.4. Other methods

Electron transport measurements reveal information about the electronic behaviour of individual nanotubes, and the effect of molecules on SWNTs can be measured as systematic changes in resistance or in p- or n-doped behaviour. Scanning tunneling microscopy (STM) and scanning tunneling spectroscopy (STS) reveal information about local changes in individual nanotubes. For example, an encapsulated molecule

can locally strain or electronically perturb a section of a nanotube sidewall, changing the tunnelling voltage in STM.

Nanotubes contacted to two electrodes with a back gate can form a basic field effect transistor (FET) or a metallic wire (Fig. 14). By studying how electronic properties of individual nanotubes are changed by interactions with different molecules, it can directly evaluated how useful the nanotube is as a wire or a transistor. Chiu *et al.*[170] reported a p- to n-type transition of an FET made of an individual (Dy@C$_{82}$)@SWNT peapod when cooled from 300 K to 265 K. Upon further cooling to 215 K, they observed metallic behaviour of the same peapod. Below 75 K Coulomb blockade behaviour was observed that resembled a series of several quantum dots formed within nanotube electronic bands. The authors suggest that the transition from p- to n-type behaviour is a result of cooling causing an increase in overlap of the Dy@C$_{82}$ orbitals with SWNT bands and charge transfer from
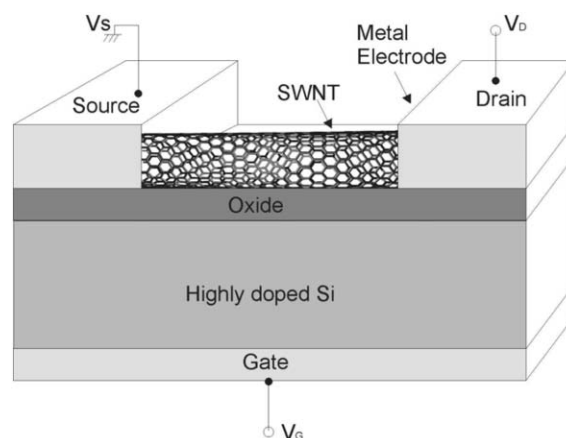

Fig. 14 Schematic representation of a single nanotube FET (courtesy of Natalie Plank).

the $Dy@C_{82}$ to the conduction band of the SWNT. Shimada *et al.*[145] reported that $C_{60}@SWNT$ peapod FETs show only p-type behaviour, whereas $(Gd@C_{82})@SWNT$ peapods display ambipolar (p- and n-type) FET behaviour. The properties of $(Gd@C_{82})@SWNT$ peapods were ascribed to the narrowing of nanotube band gap due to the interaction with metallofullerenes also observed in STM[146] and described below. Unlike Chiu *et al.*, these authors did not observe any change in the dominant carriers in $(Gd@C_{82})@SWNT$ from 23 K to room temperature. Shimada *et al.* subsequently reported a large variety of other peapod FETs filled with a range of fullerenes and metallofullerenes.[171,172] They found that all metallofullerene peapods show ambipolar FET behaviour.[172] They also found that peapods show a monotonic decrease in 'off-state' voltage width with an increase in the charge of the fullerene cage.[172] C_{60} (0 charge on the cage) peapod FETs have the largest window of gate voltage for 'off' behaviour, and $Gd_2@C_{92}$ (-6 charge on the cage) peapod FETs behave as metals, thus have no 'off' behaviour. An exception in this trend are $C_{90}@SWNTs$ peapods, which have no charge on the fullerene cage, but behave as metallic wires with no 'off' behaviour.[171] A direct assignment of a specific nanotube or peapod being measured by a combination of transport and Raman or TEM allows the effect of nanotube–electrode contact resistance to be taken into account more readily[173] and can provide more detailed understanding of how molecules affect transport behaviour and thus fundamental electronic structure of SWNTs.

There have been a few examples of locally probing SWNTs filled with fullerenes using STM and STS. Almost simultaneously, Hornbaker *et al.* reported STM/STS measurements of $C_{60}@SWNTs$[174] and Lee *et al.* reported STM/STS measurements of $(Gd@C_{82})@SWNTs$.[146] Hornbaker *et al.* observed local variations in the density of states of peapods with the spatial periodicity of C_{60} inside a SWNT.[174] They suggested from a combination of experiments and calculations that the observed hybrid electronic band arises from mixing of nanotube bands and fullerene molecular orbitals. Lee *et al.*[146] also observed that $Gd@C_{82}$ fullerenes appear as a local variation in the density of states along the nanotube axis. This effect, quantified as a bandgap narrowing of *ca.* 0.4 eV, was attributed to charge transfer and strain effect arising from metallofullerene encapsulation. The observed bandgap narrowing was invoked by Shimada *et al.* to explain the FET measurements for peapods.[145,171,172]

6. Applications of molecular nanotube architectures

As illustrated in the previous sections, many molecular species form strong but reversible interactions with carbon nanotubes which provide a basis for the most obvious application—nanotubes as sorbent material. Indeed, Long and Yang have reported that nanotubes are superior adsorbents of dioxins and nitrogen oxides.[175,176] Peng *et al.* have observed that dichlorobenzene is readily removed from waste water over a variety of pH ranges.[177] Li *et al.* have shown nanotubes to remove lead from water.[178] Srivastava *et al.* have made multiwalled nanotube filters that effectively removed heavy hydrocarbons from petroleum and *E. coli* bacteria and

poliovirus from water.[179] These applications of nanotubes as sorbents show that interactions can be strong but reversible and can work based on covalent, ionic and dispersive interactions.

Carbon nanotubes have been touted as highly sensitive molecular detectors. Kong *et al.* showed that individual semiconducting SWNTs exhibit changes in conductance of several orders of magnitude upon exposure to NO_2 or NH_3;[180] NO_2 increased conductance and NH_3 decreased conductance of SWNT FETs. The nanotube-based sensors could detect 100 ppm NO_2 in 2 to 10 seconds. As discussed in Section 3.1, both of these molecules show large IR shifts upon adsorption, indicating a strong interaction with SWNTs. By measuring the capacitance, nanotubes were found to be highly effective at detecting dimethyl methylphosphonate, a simulant for the nerve agent sarin, with the ability to detect concentrations of 50 ppb in four seconds.[181]

In addition to being able to detect molecules by changes in SWNT resistance, sensors can operate based on changes in dielectric, gravimetric, optical, and mechanical resonance changes in SWNTs.[182] Zribi *et al.* coupled SWNTs with a microelectromechanical resonator in an attempt to detect CO_2. They found a linear downshift in the resonant frequency of the device with stress induced by CO_2 adsorption on the SWNTs. They noted no substantial effect on the SWNT resonance upon exposure to 'interfering' gases H_2O and O_2. Other gas sensing applications could be developed by forming a noncovalent coating on SWNTs that selectively interact with a specific gas and change the nanotube physical properties.

Very rapid progress is being made for using SWNTs for biological applications. Barone *et al.* have shown that carbon nanotubes can be used to monitor blood glucose levels[183] using the fact that nanotubes luminesce in the near-IR, a region where the body's tissues are transparent. Implanted SWNTs coated with glucose oxidase functionalized with ferricyanide will react with glucose in the body and change their luminescent properties, which can be monitored using an external NIR detector. This method works particularly well because the glucose oxidase was not covalently bound to the SWNT surface, which would have detrimentally affected SWNT luminescence.

Single-walled nanotubes are particularly interesting for templating polymerization reactions. Gomez *et al.* showed that pyrene groups adsorbed onto the exterior of SWNTs could serve as anchors for catalyst of ring-opening polymerisation of norbornene.[77] Their work revealed that polymerisation on the exterior of a SWNT shows unique dynamics, where longer reaction times result in thinner polymer coatings. They showed that SWNTs could be coated with polymer while on a SiO_2 surface, a possible way to create insulating coatings around SWNT wires in electronic devices. We and others have demonstrated that polymerization reactions can be carried out inside SWNTs to form unique products not favourable in the bulk.[102,120,121,184] These kinds of reactions are particularly useful because the product geometry is dictated by physical confinement, which could lead to new polymeric materials.

Carbon nanotubes are already used in some commercial products. Multiwalled nanotubes are being pursued for many applications because they are cheaper to manufacture in large

This journal is © The Royal Society of Chemistry 2006

Chem. Soc. Rev., 2006, **35**, 637–659 | 655

quantities. Currently, multiwalled nanotubes are used as an electrically conductive additive to polymers, enabling electrostatic painting of plastic parts. Also, multiwalled nanotubes have been integrated into water filters that show the ability to remove bacteria and viruses. Nanotubes are being used effectively in lithium ion batteries to increase the number of cycles that the battery maintains charge. Also, the ''sharpness'' and high electrical conductivity of nanotubes make them ideal field emission sources for displays. A hydrogen gas detection device made of arrays of SWNT transistors is commercially available. Also, nanotubes are being used for transparent conductive films to replace ITO for a variety of applications, including LCDs, touch screens, and photovoltaics. Several companies are developing useful commercial applications of nanotubes for our daily lives. In almost all cases, the product involves taking advantage of an interaction between the nanotube and its environment. We expect to see more applications developing across a wide variety of industries, and we believe that understanding interactions of molecules with nanotube outer surfaces and internal cavities will be crucial to developing these applications.

7. Summary

From the examples detailed above, it appears that a molecule (either electron donating or accepting) that ionically bonds to a SWNT has little or no selectivity for the interior or exterior of the SWNT, whereas covalent bonding occurs most favourably on the exterior of the SWNT, and dispersive interactions are most highly favoured inside the SWNT cavity, provided that the nanotube is wide enough to accommodate the molecule. These observations indicate that nanotubes can selectively react, adsorb or absorb molecules based on steric constraints and the type of interaction.

Carbon nanotubes affect molecules over a wide range of energy scales, depending on the type of interaction between the molecule and nanotube. New phases of molecules occur inside SWNTs due to nanoscale confinement. Molecular dynamic behaviour and chemical reactivity are also affected by nanotubes. In turn the molecules alter the intrinsic properties of SWNTs, making these structures effective for gas sensors, nanoelectronic devices, and biological sensors.

To truly understand the effects of molecules on nanotubes and nanotubes on molecules, these hybrid materials must be studied with a combination of different spectroscopic and microscopic techniques. TEM is valuable for assigning the location molecules inside SWNTs and determining their structural features. IR spectroscopy is a sensitive tool for studying the effect of SWNTs on molecular vibrations. Thermal desorption spectroscopy gives valuable information about binding energies of molecules to SWNTs surfaces. Raman spectroscopy gives a wealth of information about both molecules and SWNTs, especially how molecules impact the SWNT vibrations. Photoluminescence and absorption spectroscopy provide information about nanotube electronic transitions and how they are altered by coupling with molecular orbitals. Using these techniques, we can gain a much deeper understanding of the mechanisms of interactions of nanotubes with molecules, which will enable further progress in development of practical applications of these fascinating materials.

References

1 R. Saito, G. Dresselhaus and M. S. Dresselhaus, *Physical Properties of Carbon Nanotubes*, Imperial College Press, London, 1998.
2 N. Wang, Z. K. Tang, G. D. Li and J. S. Chen, *Nature*, 2000, **408**, 50.
3 Q. H. Yang, S. Bai, J. L. Sauvajol and J. B. Bai, *Adv. Mater.*, 2003, **15**, 792.
4 S. Iijima, *Nature*, 1991, **354**, 56.
5 W. Kratschmer, L. D. Lamb, K. Fostiropoulos and D. R. Huffman, *Nature*, 1990, **347**, 354.
6 H. W. Kroto, J. R. Heath, S. C. Obrien, R. F. Curl and R. E. Smalley, *Nature*, 1985, **318**, 162.
7 A. Oberlin, M. Endo and T. Koyama, *J. Cryst. Growth*, 1976, **32**, 335.
8 H. G. Tennent, in *Carbon fibrils, method for producing the same and compositions containing same*, ed. U. S. P., 4,663,230, 1987.
9 S. Iijima and T. Ichihashi, *Nature*, 1993, **363**, 603.
10 D. S. Bethune, C. H. Kiang, M. S. Devries, G. Gorman, R. Savoy, J. Vazquez and R. Beyers, *Nature*, 1993, **363**, 605.
11 P. Avouris, *Acc. Chem. Res.*, 2002, **35**, 1026.
12 E. T. Thostenson, Z. F. Ren and T. W. Chou, *Compos. Sci. Technol.*, 2001, **61**, 1899.
13 M. S. Dresselhaus, K. A. Williams and P. C. Eklund, *MRS Bull.*, 1999, **24**, 45.
14 M. Monthioux, *Carbon*, 2002, **40**, 1809.
15 J. Sloan, D. E. Luzzi, A. I. Kirkland, J. L. Hutchison and M. L. H. Green, *MRS Bull.*, 2004, **29**, 265.
16 N. W. S. Kam, M. O'Connell, J. A. Wisdom and H. J. Dai, *Proc. Natl. Acad. Sci. U. S. A.*, 2005, **102**, 11600.
17 S. J. Son, J. Reichel, B. He, M. Schuchman and S. B. Lee, *J. Am. Chem. Soc.*, 2005, **127**, 7316.
18 C. R. Martin and P. Kohli, *Nat. Rev. Drug Discovery*, 2003, **2**, 29.
19 L. A. Girifalco, M. Hodak and R. S. Lee, *Phys. Rev. B: Condens. Matter*, 2000, **62**, 13104.
20 A. Thess, R. Lee, P. Nikolaev, H. Dai, P. Petit, J. Robert, C. Xu, Y. H. Lee, S. G. Kim, A. G. Rinzler, D. T. Colbert, G. E. Scuseria, D. Tomanek, J. E. Fischer and R. E. Smalley, *Science*, 1996, **273**, 483.
21 J. Chen, M. A. Hamon, H. Hu, Y. S. Chen, A. M. Rao, P. C. Eklund and R. C. Haddon, *Science*, 1998, **282**, 95.
22 A. Hirsch, *Angew. Chem., Int. Ed.*, 2002, **41**, 1853.
23 S. Niyogi, M. A. Hamon, H. Hu, B. Zhao, P. Bhowmik, R. Sen, M. E. Itkis and R. C. Haddon, *Acc. Chem. Res.*, 2002, **35**, 1105.
24 A. Rakitin, C. Papadopoulos and J. M. Xu, *Phys. Rev. B: Condens. Matter*, 2003, **67**, 033411.
25 S. M. Lee, K. H. An, Y. H. Lee, G. Seifert and T. Frauenheim, *J. Am. Chem. Soc.*, 2001, **123**, 5059.
26 Z. F. Chen, W. Thiel and A. Hirsch, *ChemPhysChem*, 2003, **4**, 93.
27 M. W. Zhao, Y. Y. Xia, Y. C. Ma, M. J. Ying, X. D. Liu and L. M. Mei, *Phys. Rev. B: Condens. Matter*, 2002, **66**, art. no. 155403.
28 A. V. Krasheninnikov, K. Nordlund, P. O. Lehtinen, A. S. Foster, A. Ayuela and R. M. Nieminen, *Carbon*, 2004, **42**, 1021.
29 M. W. Zhao, Y. Y. Xia, J. P. Lewis and L. M. Mei, *J. Phys. Chem. B*, 2004, **108**, 9599.
30 S. Banerjee and S. S. Wong, *Nano Lett.*, 2004, **4**, 1445.

31 F. Tournus and J. C. Charlier, *Phys. Rev. B: Condens. Matter*, 2005, **71**, 165421.

32 L. A. Girifalco and M. Hodak, *Phys. Rev. B: Condens. Matter*, 2002, **65**, 125404.

33 H. Ulbricht, G. Moos and T. Hertel, *Phys. Rev. Lett.*, 2003, **90**, 095501.

34 J. Breton, J. Gonzalezplatas and C. Girardet, *J. Chem. Phys.*, 1994, **101**, 3334.

35 M. Hodak and L. A. Girifalco, *Phys. Rev. B: Condens. Matter*, 2003, **67**, 075419.

36 M. Hodak and L. A. Girifalco, *Chem. Phys. Lett.*, 2001, **350**, 405.

37 K. S. Troche, V. R. Coluci, S. F. Braga, D. D. Chinellato, F. Sato, S. B. Legoas, R. Rurali and D. S. Galvao, *Nano Lett.*, 2005, **5**, 349.

38 G. Stan, M. J. Bojan, S. Curtarolo, S. M. Gatica and M. W. Cole, *Phys. Rev. B: Condens. Matter*, 2000, **62**, 2173.

39 D. J. Shu and X. G. Gong, *J. Chem. Phys.*, 2001, **114**, 10922.

40 M. W. Zhao, Y. Y. Xia and L. M. Mei, *Phys. Rev. B: Condens. Matter*, 2005, **71**, 165413.

41 J. Lu, S. Nagase, S. Zhang and L. M. Peng, *Phys. Rev. B: Condens. Matter*, 2004, **69**, 205304.

42 C. Matranga and B. Bockrath, *J. Phys. Chem. B*, 2005, **109**, 4853.

43 W. F. Du, L. Wilson, J. Ripmeester, R. Dutrisac, B. Simard and S. Denommee, *Nano Lett.*, 2002, **2**, 343.

44 M. Eswaramoorthy, R. Sen and C. N. R. Rao, *Chem. Phys. Lett.*, 1999, **304**, 207.

45 K. Hirahara, S. Bandow, K. Suenaga, H. Kato, T. Okazaki, H. Shinohara and S. Iijima, *Phys. Rev. B: Condens. Matter*, 2001, **6411**, art. no.

46 W. Teizer, R. B. Hallock, E. Dujardin and T. W. Ebbesen, *Phys. Rev. Lett.*, 1999, **82**, 5305.

47 W. Teizer, R. B. Hallock, E. Dujardin and T. W. Ebbesen, *Phys. Rev. Lett.*, 2000, **84**, 1844.

48 S. Talapatra, A. Z. Zambano, S. E. Weber and A. D. Migone, *Phys. Rev. Lett.*, 2000, **85**, 138.

49 A. J. Zambano, S. Talapatra and A. D. Migone, *Phys. Rev. B: Condens. Matter*, 2001, **64**, 075415.

50 S. E. Weber, S. Talapatra, C. Journet, Z. Zambano and A. D. Migone, *Phys. Rev. B: Condens. Matter*, 2000, **61**, 13150.

51 H. Ulbricht, J. Kriebel, G. Moos and T. Hertel, *Chem. Phys. Lett.*, 2002, **363**, 252.

52 W. Shi and J. K. Johnson, *Phys. Rev. Lett.*, 2003, **91**, 015504.

53 S. Rols, M. R. Johnson, P. Zeppenfeld, M. Bienfait, O. E. Vilches and J. Schneble, *Phys. Rev. B: Condens. Matter*, 2005, **71**, 155411.

54 W. L. Yim, O. Byl, J. T. Yates and J. K. Johnson, *J. Chem. Phys.*, 2004, **120**, 5377.

55 O. Byl, P. Kondratyuk and J. T. Yates, *J. Phys. Chem. B*, 2003, **107**, 4277.

56 C. Matranga and B. Bockrath, *J. Phys. Chem. B*, 2005, **109**, 9209.

57 M. D. Ellison, A. P. Good, C. S. Kinnaman and N. E. Padgett, *J. Phys. Chem. B*, 2005, **109**, 10640.

58 O. Byl, P. Kondratyuk, S. T. Forth, S. A. FitzGerald, L. Chen, J. K. Johnson and J. T. Yates, *J. Am. Chem. Soc.*, 2003, **125**, 5889.

59 M. D. Ellison, M. J. Crotty, D. Koh, R. L. Spray and K. E. Tate, *J. Phys. Chem. B*, 2004, **108**, 7938.

60 X. Feng, S. Irle, H. Witek, K. Morokuma, R. Vidic and E. Borguet, *J. Am. Chem. Soc.*, 2005, **127**, 10533.

61 M. K. Kostov, E. E. Santiso, A. M. George, K. E. Gubbins and M. B. Nardelli, *Phys. Rev. Lett.*, 2005, **95**, 136105.

62 J. J. Zhao, A. Buldum, J. Han and J. P. Lu, *Nanotechnology*, 2002, **13**, 195.

63 H. Chang, J. D. Lee, S. M. Lee and Y. H. Lee, *Appl. Phys. Lett.*, 2001, **79**, 3863.

64 S. Peng and K. J. Cho, *Nanotechnology*, 2000, **11**, 57.

65 W. L. Yim, X. G. Gong and Z. F. Liu, *J. Phys. Chem. B*, 2003, **107**, 9363.

66 F. Mercuri, A. Sgamellotti, L. Valentini, I. Armentano and J. M. Kenny, *J. Phys. Chem. B*, 2005, **109**, 13175.

67 G. U. Sumanasekera, B. K. Pradhan, H. E. Romero, K. W. Adu and P. C. Eklund, *Phys. Rev. Lett.*, 2002, **89**, 166801.

68 S. Banerjee, T. Hemraj-Benny and S. S. Wong, *Adv. Mater.*, 2005, **17**, 17.

69 M. J. O'Connell, S. M. Bachilo, C. B. Huffman, V. C. Moore, M. S. Strano, E. H. Haroz, K. L. Rialon, P. J. Boul, W. H. Noon, C. Kittrell, J. P. Ma, R. H. Hauge, R. B. Weisman and R. E. Smalley, *Science*, 2002, **297**, 593.

70 V. C. Moore, M. S. Strano, E. H. Haroz, R. H. Hauge, R. E. Smalley, J. Schmidt and Y. Talmon, *Nano Lett.*, 2003, **3**, 1379.

71 C. Richard, F. Balavoine, P. Schultz, T. W. Ebbesen and C. Mioskowski, *Science*, 2003, **300**, 775.

72 J. G. Wiltshire, L. J. Li, A. N. Khlobystov, C. J. Padbury, G. A. D. Briggs and R. J. Nicholas, *Carbon*, 2005, **43**, 1151.

73 L. J. Li, R. J. Nicolas, C. Y. Chen, R. C. Darton and S. C. Baker, *Nanotechnology*, 2005, **16**, S202.

74 W. Wenseleers, I. I. Vlasov, E. Goovaerts, E. D. Obraztsova, A. S. Lobach and A. Bouwen, *Adv. Funct. Mater.*, 2004, **14**, 1105.

75 M. F. Islam, E. Rojas, D. M. Bergey, A. T. Johnson and A. G. Yodh, *Nano Lett.*, 2003, **3**, 269.

76 R. J. Chen, Y. G. Zhan, D. W. Wang and H. J. Dai, *J. Am. Chem. Soc.*, 2001, **123**, 3838.

77 F. J. Gomez, R. J. Chen, D. W. Wang, R. M. Waymouth and H. J. Dai, *Chem. Commun.*, 2003, 190.

78 J. Zhang, J. K. Lee, Y. Wu and R. W. Murray, *Nano Lett.*, 2003, **3**, 403.

79 X. B. Wang, Y. Q. Liu, W. F. Qiu and D. B. Zhu, *J. Mater. Chem.*, 2002, **12**, 1636.

80 H. P. Li, B. Zhou, Y. Lin, L. R. Gu, W. Wang, K. A. S. Fernando, S. Kumar, L. F. Allard and Y. P. Sun, *J. Am. Chem. Soc.*, 2004, **126**, 1014.

81 M. J. O'Connell, P. Boul, L. M. Ericson, C. Huffman, Y. H. Wang, E. Haroz, C. Kuper, J. Tour, K. D. Ausman and R. E. Smalley, *Chem. Phys. Lett.*, 2001, **342**, 265.

82 M. Zheng, A. Jagota, E. D. Semke, B. A. Diner, R. S. McLean, S. R. Lustig, R. E. Richardson and N. G. Tassi, *Nat. Mater.*, 2003, **2**, 338.

83 A. Star, J. F. Stoddart, D. Steuerman, M. Diehl, A. Boukai, E. W. Wong, X. Yang, S. W. Chung, H. Choi and J. R. Heath, *Angew. Chem., Int. Ed.*, 2001, **40**, 1721.

84 M. I. H. Panhuis, A. Maiti, A. B. Dalton, A. van den Noort, J. N. Coleman, B. McCarthy and W. J. Blau, *J. Phys. Chem. B*, 2003, **107**, 478.

85 K. Suenaga, R. Taniguchi, T. Shimada, T. Okazaki, H. Shinohara and S. Iijima, *Nano Lett.*, 2003, **3**, 1395.

86 A. C. Dillon, K. M. Jones, T. A. Bekkedahl, C. H. Kiang, D. S. Bethune and M. J. Heben, *Nature*, 1997, **386**, 377.

87 B. W. Smith, M. Monthioux and D. E. Luzzi, *Nature*, 1998, **396**, 323.

88 E. Dujardin, T. W. Ebbesen, H. Hiura and K. Tanigaki, *Science*, 1994, **265**, 1850.

89 T. W. Ebbesen, *J. Phys. Chem. Solids*, 1996, **57**, 951.

90 S. Berber, Y. K. Kwon and D. Tomanek, *Phys. Rev. Lett.*, 2002, **88**, 185502.

91 H. Ulbricht and T. Hertel, *J. Phys. Chem. B*, 2003, **107**, 14185.

92 M. Hodak and L. A. Girifalco, *Phys. Rev. B: Condens. Matter*, 2001, **6403**, 035407.

93 O. Dubay and G. Kresse, *Phys. Rev. B: Condens. Matter*, 2004, **70**, art. no 165424.

94 K. Hirahara, K. Suenaga, S. Bandow, H. Kato, T. Okazaki, H. Shinohara and S. Iijima, *Phys. Rev. Lett.*, 2000, **85**, 5384.

95 D. E. Luzzi and B. W. Smith, *Carbon*, 2000, **38**, 1751.

96 M. Yudasaka, K. Ajima, K. Suenaga, T. Ichihashi, A. Hashimoto and S. Iijima, *Chem. Phys. Lett.*, 2003, **380**, 42.

97 F. Simon, H. Kuzmany, H. Rauf, T. Pichler, J. Bernardi, H. Peterlik, L. Korecz, F. Fulop and A. Janossy, *Chem. Phys. Lett.*, 2004, **383**, 362.

98 A. N. Khlobystov, D. A. Britz, J. W. Wang, S. A. O'Neil, M. Poliakoff and G. A. D. Briggs, *J. Mater. Chem.*, 2004, **14**, 2852.

99 D. A. Britz, A. N. Khlobystov, J. W. Wang, A. S. O'Neil, M. Poliakoff, A. Ardavan and G. A. Briggs, *Chem. Commun.*, 2004, 176.

100 D. A. Morgan, J. Sloan and M. L. H. Green, *Chem. Commun.*, 2002, 2442.

101 L. J. Li, A. N. Khlobystov, J. G. Wiltshire, G. A. D. Briggs and R. J. Nicholas, *Nat. Mater.*, 2005, **4**, 481.

102 Y. Fujita, S. Bandow and S. Iijima, *Chem. Phys. Lett.*, 2005, **413**, 410.

This journal is © The Royal Society of Chemistry 2006

Chem. Soc. Rev., 2006, **35**, 637–659 | 657

103 J. Sloan, A. I. Kirkland, J. L. Hutchison and M. L. H. Green, *Acc. Chem. Res.*, 2002, **35**, 1054.
104 A. N. Khlobystov, D. A. Britz, A. Ardavan and G. A. D. Briggs, *Phys. Rev. Lett.*, 2004, **92**, 245507.
105 S. Okada, S. Saito and A. Oshiyama, *Phys. Rev. Lett.*, 2001, **86**, 3835.
106 A. N. Khlobystov, R. Scipioni, D. Nguyen-Manh, D. A. Britz, D. G. Pettifor, G. A. D. Briggs, S. G. Lyapin, A. Ardavan and R. J. Nicholas, *Appl. Phys. Lett.*, 2004, **84**, 792.
107 L. H. Guan, H. J. Li, Z. J. Shi, L. P. You and Z. N. Gu, *Solid State Commun.*, 2005, **133**, 333.
108 G. Hummer, J. C. Rasaiah and J. P. Noworyta, *Nature*, 2001, **414**, 188.
109 K. Koga, G. T. Gao, H. Tanaka and X. C. Zeng, *Nature*, 2001, **412**, 802.
110 W. H. Noon, K. D. Ausman, R. E. Smalley and J. P. Ma, *Chem. Phys. Lett.*, 2002, **355**, 445.
111 R. J. Mashl, S. Joseph, N. R. Aluru and E. Jakobsson, *Nano Lett.*, 2003, **3**, 589.
112 Y. Maniwa, H. Kataura, M. Abe, S. Suzuki, Y. Achiba, H. Kira and K. Matsuda, *J. Phys. Soc. Jpn.*, 2002, **71**, 2863.
113 Y. Maniwa, H. Kataura, M. Abe, A. Udaka, S. Suzuki, Y. Achiba, H. Kira, K. Matsuda, H. Kadowaki and Y. Okabe, *Chem. Phys. Lett.*, 2005, **401**, 534.
114 A. I. Kolesnikov, J. M. Zanotti, C. K. Loong, P. Thiyagarajan, A. P. Moravsky, R. O. Loutfy and C. J. Burnham, *Phys. Rev. Lett.*, 2004, **93**, 035503.
115 B. W. Smith, D. E. Luzzi and Y. Achiba, *Chem. Phys. Lett.*, 2000, **331**, 137.
116 K. Suenaga, T. Okazaki, C. R. Wang, S. Bandow, H. Shinohara and S. Iijima, *Phys. Rev. Lett.*, 2003, **90**, 055506.
117 A. N. Khlobystov, K. Porfyrakis, M. Kanai, D. A. Britz, A. Ardavan, H. Shinohara, T. J. S. Dennis and G. A. D. Briggs, *Angew. Chem., Int. Ed.*, 2004, **43**, 1386.
118 M. D. Halls and K. Raghavachari, *Nano Lett.*, 2005, **5**, 1861.
119 S. Bandow, K. Hirahara, T. Hiraoka, G. Chen, P. Eklund and S. Iijima, *MRS Bull.*, 2004, **29**, 260.
120 D. A. Britz, A. N. Khlobystov, K. Porfyrakis, A. Ardavan and G. A. D. Briggs, *Chem. Commun.*, 2005, 37.
121 T. Pichler, H. Kuzmany, H. Kataura and Y. Achiba, *Phys. Rev. Lett.*, 2001, **8726**, art. no. 267401.
122 X. Liu, T. Pichler, M. Knupfer, J. Fink and H. Kataura, *Phys. Rev. B: Condens. Matter*, 2004, **69**, 075417.
123 X. Fan, E. C. Dickey, P. C. Eklund, K. A. Williams, L. Grigorian, R. Buczko, S. T. Pantelides and S. J. Pennycook, *Phys. Rev. Lett.*, 2000, **84**, 4621.
124 L. Grigorian, K. A. Williams, S. Fang, G. U. Sumanasekera, A. L. Loper, E. C. Dickey, S. J. Pennycook and P. C. Eklund, *Phys. Rev. Lett.*, 1998, **80**, 5560.
125 C. H. Turner, J. K. Johnson and K. E. Gubbins, *J. Chem. Phys.*, 2001, **114**, 1851.
126 Y. L. Zhao, M. D. Bartberger, K. Goto, K. Shimada, T. Kawashima and K. N. Houk, *J. Am. Chem. Soc.*, 2005, **127**, 7964.
127 M. S. Dresselhaus, G. Dresselhaus, R. Saito and A. Jorio, *Phys. Rep.*, 2005, **409**, 47.
128 S. Bandow, M. Takizawa, H. Kato, T. Okazaki, H. Shinohara and S. Iijima, *Chem. Phys. Lett.*, 2001, **347**, 23.
129 X. Liu, T. Pichler, M. Knupfer, M. S. Golden, J. Fink, H. Kataura, Y. Achiba, K. Hirahara and S. Iijima, *Phys. Rev. B: Condens. Matter*, 2002, **65**, 045419.
130 B. W. Smith, R. M. Russo, S. B. Chikkannanavar and D. E. Luzzi, *J. Appl. Phys.*, 2002, **91**, 9333.
131 V. Skákalová, A. B. Kaiser, U. Dettlaff-Weglikowska, K. Hrncarikova and S. Roth, *J. Phys. Chem. B*, 2005, **109**, 7174.
132 G. G. Chen, C. A. Furtado, S. Bandow, S. Iijima and P. C. Eklund, *Phys. Rev. B: Condens. Matter*, 2005, **71**, 045408.
133 A. M. Rao, P. C. Eklund, S. Bandow, A. Thess and R. E. Smalley, *Nature*, 1997, **388**, 257.
134 J. Sandler, M. S. P. Shaffer, A. H. Windle, M. P. Halsall, M. A. Montes-Moran, C. A. Cooper and R. J. Young, *Phys. Rev. B: Condens. Matter*, 2003, **67**, 035417.
135 J. R. Wood, M. D. Frogley, E. R. Meurs, A. D. Prins, T. Peijs, D. J. Dunstan and H. D. Wagner, *J. Phys. Chem. B*, 1999, **103**, 10388.
136 U. D. Venkateswaran, A. M. Rao, E. Richter, M. Menon, A. Rinzler, R. E. Smalley and P. C. Eklund, *Phys. Rev. B: Condens. Matter*, 1999, **59**, 10928.
137 J. R. Wood and H. D. Wagner, *Appl. Phys. Lett.*, 2000, **76**, 2883.
138 J. R. Wood, Q. Zhao, M. D. Frogley, E. R. Meurs, A. D. Prins, T. Peijs, D. J. Dunstan and H. D. Wagner, *Phys. Rev. B: Condens. Matter*, 2000, **62**, 7571.
139 S. B. Cronin, A. K. Swan, M. S. Unlu, B. B. Goldberg, M. S. Dresselhaus and M. Tinkham, *Phys. Rev. Lett.*, 2004, **93**, 167401.
140 S. B. Cronin, A. K. Swan, M. S. Unlu, B. B. Goldberg, M. S. Dresselhaus and M. Tinkham, *Phys. Rev. B: Condens. Matter*, 2005, **72**, 035425.
141 M. Yoon, S. Berber and D. Tomanek, *Phys. Rev. B: Condens. Matter*, 2005, **71**, 155406.
142 H. Shinohara, *Rep. Prog. Phys.*, 2000, **63**, 843.
143 P. W. Chiu, S. F. Yang, S. H. Yang, G. Gu and S. Roth, *Appl. Phys. A: Mater. Sci. Process.*, 2003, **76**, 463.
144 Y. M. Cho, S. W. Han, G. Kim, H. Lee and J. Ihm, *Phys. Rev. Lett.*, 2003, **90**, 106402.
145 T. Shimada, T. Okazaki, R. Taniguchi, T. Sugai, H. Shinohara, K. Suenaga, Y. Ohno, S. Mizuno, S. Kishimoto and T. Mizutani, *Appl. Phys. Lett.*, 2002, **81**, 4067.
146 J. Lee, H. Kim, S. J. Kahng, G. Kim, Y. W. Son, J. Ihm, H. Kato, Z. W. Wang, T. Okazaki, H. Shinohara and Y. Kuk, *Nature*, 2002, **415**, 1005.
147 A. Debarre, R. Jaffiol, C. Julien, D. Nutarelli, A. Richard and P. Tchenio, *Phys. Rev. Lett.*, 2003, **91**, 085501.
148 D. A. Britz, A. N. Khlobystov, G. A. D. Briggs and A. Ardavan, *Phys. Rev. Lett.*, 2004, **93**, 269601.
149 A. Debarre, R. Jaffiol, C. Julien, D. Nutarelli, A. Richard and P. Tchenio, *Phys. Rev. Lett.*, 2004, **93**, 269602.
150 H. Kataura, Y. Maniwa, M. Abe, A. Fujiwara, T. Kodama, K. Kikuchi, H. Imahori, Y. Misaki, S. Suzuki and Y. Achiba, *Appl. Phys. A: Mater. Sci. Process.*, 2002, **74**, 349.
151 F. D'Souza and O. Ito, *Coord. Chem. Rev.*, 2005, **249**, 1410.
152 D. M. Guldi, H. Taieb, G. M. A. Rahman, N. Tagmatarchis and M. Prato, *Adv. Mater.*, 2005, **17**, 871.
153 D. M. Guldi, G. M. A. Rahman, N. Jux, N. Tagmatarchis and M. Prato, *Angew. Chem., Int. Ed.*, 2004, **43**, 5526.
154 D. M. Guldi, G. N. A. Rahman, J. Ramey, M. Marcaccio, D. Paolucci, F. Paolucci, S. H. Qin, W. T. Ford, D. Balbinot, N. Jux, N. Tagmatarchis and M. Prato, *Chem. Commun.*, 2004, 2034.
155 F. Wurthner, *Chem. Commun.*, 2004, 1564.
156 A. B. Dalton, C. Stephan, J. N. Coleman, B. McCarthy, P. M. Ajayan, S. Lefrant, P. Bernier, W. J. Blau and H. J. Byrne, *J. Phys. Chem. B*, 2000, **104**, 10012.
157 S. Kazaoui, N. Minami, R. Jacquemin, H. Kataura and Y. Achiba, *Phys. Rev. B: Condens. Matter*, 1999, **60**, 13339.
158 P. Petit, C. Mathis, C. Journet and P. Bernier, *Chem. Phys. Lett.*, 1999, **305**, 370.
159 E. Jouguelet, C. Mathis and P. Petit, *Chem. Phys. Lett.*, 2000, **318**, 561.
160 T. Takenobu, T. Takano, M. Shiraishi, Y. Murakami, M. Ata, H. Kataura, Y. Achiba and Y. Iwasa, *Nat. Mater.*, 2003, **2**, 683.
161 V. Meunier and B. G. Sumpter, *J. Chem. Phys.*, 2005, **123**, 024705.
162 J. Lu, S. Nagase, D. P. Yu, H. Q. Ye, R. S. Han, Z. X. Gao, S. Zhang and L. M. Peng, *Phys. Rev. Lett.*, 2004, **93**, 116804.
163 M. Shiraishi, S. Swaraj, T. Takenobu, Y. Iwasa, M. Ata and W. E. S. Unger, *Phys. Rev. B: Condens. Matter*, 2005, **71**, 125419.
164 L. Kavan, L. Dunsch, H. Kataura, A. Oshiyama, M. Otani and S. Okada, *J. Phys. Chem. B*, 2003, **107**, 7666.
165 M. S. Strano, C. B. Huffman, V. C. Moore, M. J. O'Connell, E. H. Haroz, J. Hubbard, M. Miller, K. Rialon, C. Kittrell, S. Ramesh, R. H. Hauge and R. E. Smalley, *J. Phys. Chem. B*, 2003, **107**, 6979.
166 L. J. Li and R. J. Nicholas, *Nanotechnology*, 2004, **15**, 1844.
167 H. Hu, B. Zhao, M. A. Hamon, K. Kamaras, M. E. Itkis and R. C. Haddon, *J. Am. Chem. Soc.*, 2003, **125**, 14893.
168 J. Lefebvre, J. M. Fraser, Y. Homma and P. Finnie, *Appl. Phys. A: Mater. Sci. Process.*, 2004, **78**, 1107.

169 T. Hertel, A. Hagen, V. Talalaev, K. Arnold, F. Hennrich, M. Kappes, S. Rosenthal, J. McBride, H. Ulbricht and E. Flahaut, *Nano Lett.*, 2005, **5**, 511.

170 P. W. Chiu, G. Gu, G. T. Kim, G. Philipp, S. Roth, S. F. Yang and S. Yang, *Appl. Phys. Lett.*, 2001, **79**, 3845.

171 T. Shimada, Y. Ohno, T. Okazaki, T. Sugai, K. Suenaga, S. Kishimoto, T. Mizutani, T. Inoue, R. Taniguchi, N. Fukui, H. Okubo and H. Shinohara, *Physica E*, 2004, **21**, 1089.

172 T. Shimada, Y. Ohno, K. Suenaga, T. Okazaki, S. Kishimoto, T. Mizutani, R. Taniguchi, H. Kato, B. P. Cao, T. Sugai and H. Shinohara, *Jpn. J. Appl. Phys. Part 1 – Regul. Pap. Short Notes Rev. Pap.*, 2005, **44**, 469.

173 J. C. Meyer, D. Obergfell, S. Roth, S. H. Yang and S. F. Yang, *Appl. Phys. Lett.*, 2004, **85**, 2911.

174 D. J. Hornbaker, S. J. Kahng, S. Misra, B. W. Smith, A. T. Johnson, E. J. Mele, D. E. Luzzi and A. Yazdani, *Science*, 2002, **295**, 828.

175 R. Q. Long and R. T. Yang, *J. Am. Chem. Soc.*, 2001, **123**, 2058.

176 R. Q. Long and R. T. Yang, *Ind. Eng. Chem. Res.*, 2001, **40**, 4288.

177 X. J. Peng, Y. H. Li, Z. K. Luan, Z. C. Di, H. Y. Wang, B. H. Tian and Z. P. Jia, *Chem. Phys. Lett.*, 2003, **376**, 154.

178 Y. H. Li, S. G. Wang, J. Q. Wei, X. F. Zhang, C. L. Xu, Z. K. Luan, D. H. Wu and B. Q. Wei, *Chem. Phys. Lett.*, 2002, **357**, 263.

179 A. Srivastava, O. N. Srivastava, S. Talapatra, R. Vajtai and P. M. Ajayan, *Nat. Mater.*, 2004, **3**, 610.

180 J. Kong, N. R. Franklin, C. W. Zhou, M. G. Chapline, S. Peng, K. J. Cho and H. J. Dai, *Science*, 2000, **287**, 622.

181 E. S. Snow, F. K. Perkins, E. J. Houser, S. C. Badescu and T. L. Reinecke, *Science*, 2005, **307**, 1942.

182 A. Zribi, A. Knobloch and R. Rao, *Appl. Phys. Lett.*, 2005, **86**, 203112.

183 P. W. Barone, S. Baik, D. A. Heller and M. S. Strano, *Nat. Mater.*, 2005, **4**, 86.

184 S. Bandow, M. Takizawa, K. Hirahara, M. Yudasaka and S. Iijima, *Chem. Phys. Lett.*, 2001, **337**, 48.

185 M. D. Halls and H. B. Schlegel, *J. Phys. Chem. B*, 2002, **106**, 1921.

186 L. H. Guan, K. Suenaga, Z. J. Shi, Z. N. Gu and S. Iijima, *Phys. Rev. Lett.*, 2005, **94**, 045502.

187 A. N. Khlobystov, D. A. Britz and G. A. D. Briggs, *Acc. Chem. Res.*, 2005, **38**, 901.

This journal is © The Royal Society of Chemistry 2006

Chem. Soc. Rev., 2006, **35**, 637–659 | 659